

NUS-600

MID-TERM REPORT  
FOR  
UNMANNED SPACECRAFT  
RTG SHIELD OPTIMIZATION  
STUDY

For

NATIONAL AERONAUTICS AND  
SPACE ADMINISTRATION  
GODDARD SPACE FLIGHT CENTER  
GREENBELT, MARYLAND

CONTRACT NAS5-11649

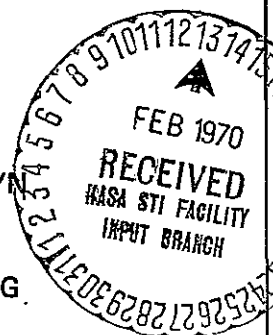
NUS CORPORATION

By

J. J. STEYN

&

R. HUANG



August 1969

NUS CORPORATION  
2351 Research Boulevard  
Rockville, Maryland 20850

FACILITY FORM 602

N70-19292

(ACCESSION NUMBER)

63

(PAGES)

CR# 108225

(NASA CR OR TMX OR AD NUMBER)

(THRU)

1

(CODE)

31

(CATEGORY)

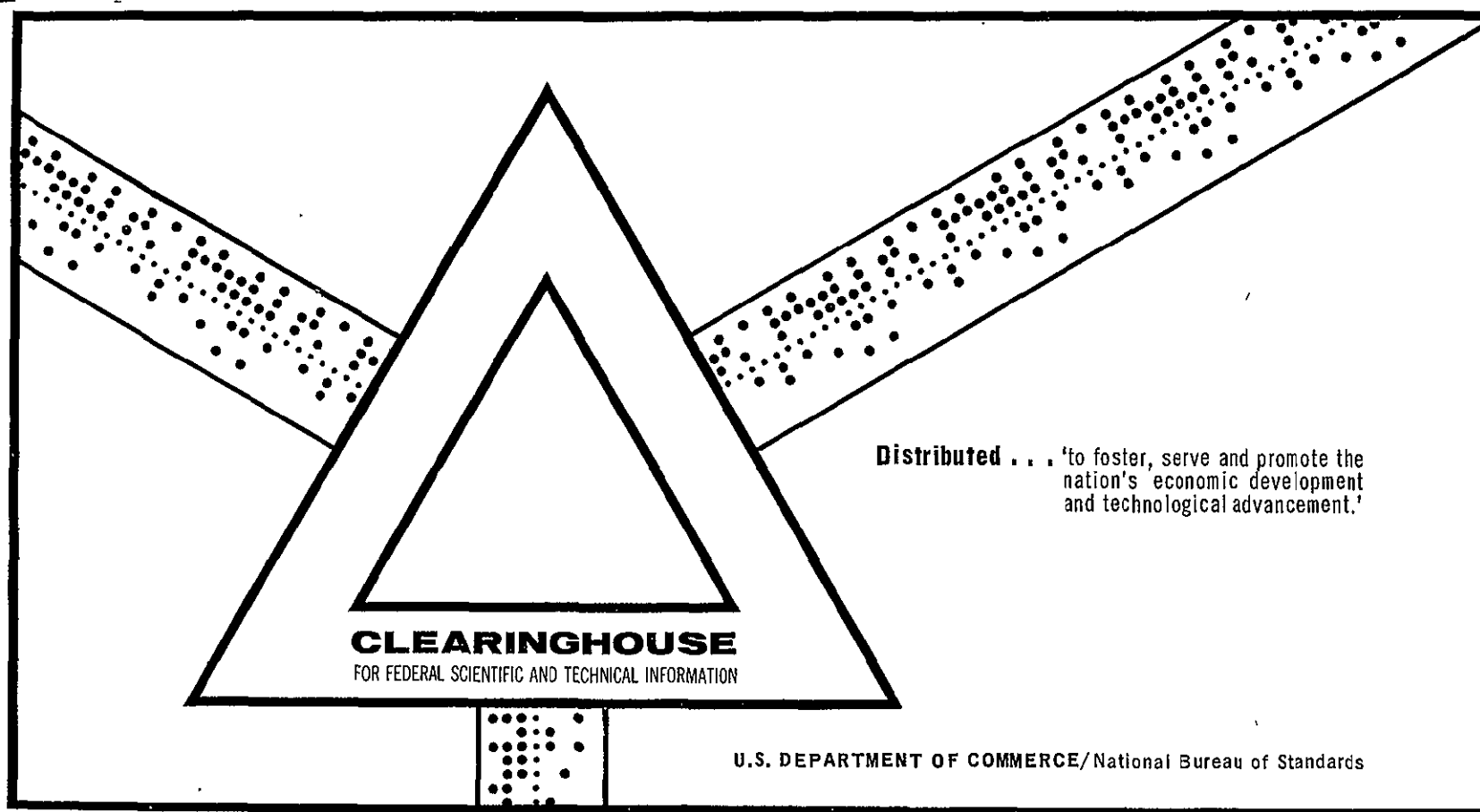
Reproduced by the  
CLEARINGHOUSE  
for Federal Scientific & Technical  
Information Springfield Va. 22151

MID-TERM REPORT FOR UNMANNED SPACECRAFT RTG SHIELD  
OPTIMIZATION STUDY

J. J. Steyn, et al.

NUS Corporation  
Rockville, Maryland

August 1969



MID-TERM REPORT FOR UNMANNED  
SPACECRAFT RTG SHIELD OPTIMIZATION STUDY

For

Goddard Space Flight Center  
Greenbelt, Maryland

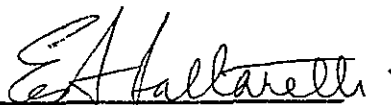
NASA Contract Number: NAS5-11649

By

J. J. Steyn & R. Huang

August 1969

NUS CORPORATION  
2351 Research Boulevard  
Rockville, Maryland 20850

Approved:   
E. A. Saltarelli  
Vice President and Manager  
Plant Engineering

## TABLE OF CONTENTS

	<u>Page</u>
I. INTRODUCTION	1
2. CODE DESCRIPTION	
2.1 Introduction	3
2.2 Theory	3
2.3 Code Logic	12
2.4 Discussion	16
3. REMAINING WORK PROGRAM	25
REFERENCES	26
FIGURES	29
TABLES	39
APPENDIX	45

## LIST OF FIGURES

<u>Figure No.</u>	<u>Title</u>	<u>Page</u>
1	Unmanned Spacecraft	30
2	Schematic Drawing of Spacecraft Showing RTG Source, Shield and Detector Arrangement	31
3	Schematic Definition of Gamma Photon and Neutron Fluxes	32
4	Code SØSC Logic	33
5	Schematic Drawing of Spacecraft Showing Specific Structural Members	34
6	Boom Scatter Intensity as a Function of Source-to-Boom Distance	35
7	NaI(Tl) Scintillation Spectra Showing Gamma Photon Scatter Distribution as a Function of Scattering Material Thickness	36
8	NaI(Tl) Scintillation Spectra Showing Gamma Photon Scatter Distribution as a Function of Incident-Angle, $\theta_0$	37
9	Energy-Integrated Angular Distribution of Shield Scattered Gamma Photons	38

## SUMMARY

This contract mid-term report discusses the progress of development of analytic procedures and computer codes for prediction of weight optimized radioisotope thermal generator shields for unmanned spacecraft operating 'in vacuo'. Optimization code - - - SØSC, designed to determine shield optimum weights and dimensions with respect to specified criterion fast neutron plus gamma photon fluxes, is described. The code employs a combination of analytic, albedo and Monte Carlo techniques. A theoretical discussion and example predicted shield data are given.

The work effort required to complete the contract program is reviewed.

## 1. INTRODUCTION

This mid-term report, prepared for the National Aeronautics and Space Administration, Goddard Space Flight Center, by NUS CORPORATION, under contract NAS5-11649, discusses the progress of development of analytic procedures and computer codes for prediction of weight optimized radiation shields for an unmanned spacecraft operating 'in vacuo'.

The work effort has been specifically oriented to the radiation field at the energetic particle experiment package indicated in the spacecraft configuration of Figure 1. Spacecraft general dimensions, deployment distances and materials were obtained from preliminary design drawings furnished by NASA-GSFC. The work has considered the radioisotope generators (RTG's) as being plutonium-oxide fuelled, viz. the SNAP-27 RTG. Although the source gamma photon and fast neutron angular-energy spectrum will be furnished by NASA-GSFC, a number and energy distribution has been assumed based on SNAP-27 and PuO<sub>2</sub> published data.

A shield optimization study code --- SØSC was designed to determine the material thickness and weight required to limit the spacecraft mission experiment package to a radiation flux exposure of  $\leq 10$  particles/cm<sup>2</sup>-sec. The incident flux was considered as being the sum of gamma photons and neutrons either transmitted by the shield or scattered by the spacecraft structure.

Code SØSC will predict shield requirements for the case of gamma photons, according to a combination of analytic particle transmission theory, the Monte Carlo transport method and the albedo technique (backscattering theory). It will employ three component sub-codes for this determination,

namely: XEST, NUGAM1 and ALB. Preliminary versions of these codes are presently designed, debugged and operational.

Although code SØSC is provisionally designed to evaluate fast neutron transport in a manner similar to that for gamma photons, it was concurred early in the present contract work to focus on photon transport in this stage of the NASA program. The code is presently designed to evaluate neutron transport using relaxation theory methods. This course for the case of the SNAP-27 is substantiated by the fact that the RTG total neutron emission rate in the axially perpendicular direction is reported as being  $5.7 \times 10^7$  n/sec<sup>(1)</sup>. This is in good agreement with, but less than an earlier NUS estimate of  $1.0 \times 10^8$  n/sec (progress report #1 attachment). Taking the gamma photon dose rate as one-tenth of the neutron dose rate and allowing for dose-to-flux conversion as well as spectral distribution gives an integrated RTG emitted photon source strength of  $\sim 1.0 \times 10^9$  γ/sec, or approximately ten times that for neutrons.

Section 2 of this report describes the theory underlying code SØSC, a description of the code and some observations resulting from preliminary data determined by the code. Section 3 discusses the work program for the remainder of the contract period.



## 2. CODE DESCRIPTION

### 2.1 Introduction

This report section describes the general theory, logic and discusses preliminary results obtained using SØSC, a code written in the FORTRAN-IV language for the NASA-GSFC IBM-360/91 digital computer. Code SØSC presently consists of three provisionally operational component codes: XEST, NUGAM1 and ALB. The reference here to provisional means that although these sub-codes are presently operational, they are not yet tested to their complete designed capability. Code XEST predicts approximate shield dimensions based on analytic methods. Code NUGAM1 predicts shield build-up factors for final shield dimensions, by the Monte Carlo method. Code ALB determines flux intensities resulting from scattering by the spacecraft structure, by means of the albedo technique.

### 2.2 Theory

For the purposes of this section the complex spacecraft configuration shown in Figure 1 is redrawn schematically in Figure 2. Only one RTG source is indicated and the mission experiment package is referred to as a detector. In addition, the spacecraft body is replaced by a simpler geometry and the boom-arms omitted.

The radiation number flux at a detector distant  $r_0$  from a source  $S$  ( $E_0$ ), of neutrons or gamma photons  $E_0$ , as in Figure 2, without a shadow shield, may be defined as

$$\phi_D(E_D) = \phi_a(E_0) + \phi_o(E_0) \quad , \quad (1)$$

where

$$\phi_{\alpha}(E_{\alpha}) = \phi_{\alpha S}(E_{\alpha S}) + \phi_{\alpha R}(E_{\alpha R}) ,$$

$\phi_{\alpha S}(E_{\alpha S})$  = the primary radiation number scattered to the detector by the area A composed of material j, distant  $r_1$  and  $r_2$  from the source and detector, respectively,

$\phi_{\alpha R}(E_{\alpha R})$  = the 'area A'-originating reaction product flux reaching the detector,

= 0, for gamma photons as the primary radiation, excepting photoneutron interactions ( $\gamma, n$ ),

$\phi_0(E_0)$  = the uncollided primary radiation number reaching the detector.

The energy arguments signify that the detected flux consists of radiation of primary energy  $E_0$ , scattered energies  $E_{\alpha S} (< E_0)$  and reaction product energies,  $E_R$ . The subscript  $\alpha$  refers to the spacecraft structure as a secondary source, eg. scattering, i.e. to albedo fluxes.

The number flux reaching the detector with a shadow shield, composed of material i, as indicated in Figure 2, may be defined as

$$\phi_D(E_D) = \phi_{\alpha}(E_{\alpha}) + \phi_a(E_0; E_a) , \quad (2)$$

where

$\phi_a(E_0; E_a)$  = the shield attenuated flux,

$$= \phi_a(E_0) + \phi_a(E_a) ,$$

$\phi_a(E_0)$  = the number flux transmitted by the shield without interaction,

$$\phi_a(E_a) = \phi_{as}(E_{as}) + \phi_{ap}(E_{ap}) + \phi_{aR}(E_{aR}),$$

$\phi_{as}(E_{as})$  = the shield forward scattered radiation number flux reaching the detector,

$\phi_{ap}(E_{ap})$  = the gamma photon number flux resulting from pair production interactions in the shield,

= 0, for incident photon energies  $E_0 \leq 1.02$  MeV,

= 0, for incident neutrons,

$\phi_{aR}(E_{aR})$  = the shield-originating reaction product number flux reaching the detector, e.g. gamma photons resulting from  $(n, \gamma)$  interactions,

= 0, generally, for gamma photons as the primary radiation, excepting such as photoneutron interactions, i.e.  $(\gamma, n)$ .

For fast neutrons as the primary incident radiation, the number flux terms

$\phi_{aR}(E_{aR})$  and  $\phi_{aR}(E_{aR})$  in Equation (1) and (2) refers to all product radiations, eg. neutrons, gamma photons, alphas, protons, depending on the reaction probabilities for each.

The number flux terms in Equations (1) and (2) may be estimated either from a combination of analytic relationships and published empirical data or from experiment, either numerical analogue, ie. Monte Carlo method or the conventional laboratory kind. The sole use of the Monte Carlo method is considered as being uneconomical and unjustified. A laboratory experiment is planned for the future by NASA-GSFC as part of the overall program. The present work is thus confined to number flux predictions obtained by analytic methods and by published empirical data and judicious use of Monte Carlo techniques.

Neglecting the reaction product number flux terms for the present, the detector incident number flux may be written as

$$\phi_D (E_D) = \phi_a (E_O) + \phi_a (E_a) + \phi_{\alpha s} (E_{\alpha s}) . \quad (3)$$

For a normally incident parallel radiation flux  $\phi_O(E_O)$ , the uncollided number flux transmitted through a shield of thickness L and reaching the detector, is obtained as

$$\phi_a (E_O) = \phi_O (E_O) e^{-\mu(E_O) \cdot L} \quad (4)$$

where

$\mu (E_O)$  = the total linear attenuation coefficient of the shield material for radiation of energy  $E_O$ ; the notation  $\Sigma$  is generally used for neutrons.

The ratio of the shield total-to-uncollided transmitted flux is referred to as "build-up". The build-up factor may thus be defined as

$$B (E_O, L) = \frac{\phi_a (E_O) + \phi_a (E_a)}{\phi_a (E_O)} = \frac{\phi_a (E_O, E_a)}{\phi_a (E_O)} . \quad (5)$$

The total shield transmitted flux at the detector may be obtained from Equations (4) and (5) as

$$\phi_a (E_O; E_a) = B (E_O, L) \cdot \phi_O (E_O) \cdot e^{-\mu(E_O) \cdot L} , \quad (6)$$

if the build-up factor is known.

Although energy and dose build-up factors may be obtained for gamma photons<sup>(2,3)</sup> and to a lesser degree for fast-neutrons they pertain in almost all cases to semi-infinite single-material-composition shields. For small finite shields, i.e. shadow shields, and number flux requirements as opposed to energy and dose, recourse

to either a laboratory experiment or a Monte Carlo study is a prerequisite. In the present work a Monte Carlo evaluation is underway for gamma photons and proposed for fast-neutrons. As noted in Section 2.4, the number build-up factor for photons was predicted as:  $1 \leq B \leq 2$ , for  $\mu L < 4$ , even for low atomic number materials.

For a spectrum of incident source particle energies the shield transmitted flux is obtained by integration as

$$\Phi_a(E_a) = \int_0^\infty \phi_a(E_o, E_a) dE_o \quad (7)$$

$$\approx \sum_{k=1}^q \phi_a(E_{ok}, E_a) \Delta E_k \quad (8)$$

For a stratified or homogenous shield composed of  $m$  materials, each of thickness  $\ell_i$ , Equation (8) may be rewritten

$$\Phi_a(E_a) \approx \sum_{k=1}^q \phi_o(E_{ok}) \prod_{i=1}^m B(E_o, \ell_i) e^{-\mu_i(E_{ok})\ell_i} \quad (9)$$

$$= \sum_{k=1}^q \phi_o(E_{ok}) \cdot B(E_o)_m \prod_{i=1}^m e^{-\mu_i(E_{ok}) \cdot \ell_i} \quad (10)$$

where

$B(E_o)_m$  = the build-up factor for the composite shield  
of  $m$  materials and incident radiation of  
energy  $E_o$ , and given geometry,

$i$  = material identity index.

The uncollided number flux in the foregoing equations may be determined from a relationship of the kind

$$\phi_o(E_o) = \phi_o(E_o, r_o) = S(E_o) \cdot G(r_o) \quad (11)$$

where

$S(E_0)$  = source emission rate for radiation of energy  $E_0$ ,

$G(r_0)$  = the geometry relationship for a source-to-detector distance  $r_0$ .

For example, for an isotropically emitting point source and  $r_0 \gg$  detector lateral extent, the geometry factor is

$$G(r_0) = (4\pi r_0^2)^{-1} \quad (12)$$

Extended source and detector geometries may be evaluated according to the 'Point-Kernel Method' <sup>(2)</sup>.

The number flux term,  $\phi_{\alpha s}(E_{\alpha s})$  in Equation (3), resulting from primary gamma photons scattered by an area  $A$ , as in Figure 2, may be redefined as

$$\phi_{\alpha s}(E_{\alpha s}) = \int_A \phi_{\alpha s}(E_0, \theta, \theta_0, \varphi, r_1, r_2, t; i) dA, \quad (13)$$

where

$dA$  = the differential scattering area,

$\theta_0$  = the angle between the incident radiation direction and the outward normal of area  $dA$ ,

$\theta$  = the angle between the emergent (scattered) radiation direction and the outward normal of area  $dA$ ,

$\varphi$  = the azimuth angle of scattering in the plane of area  $A$ ,

$r_1$  = the distance between the source and the area  $dA$ ,

$r_2$  = the distance between the area  $dA$  and the detector,

$t$  = the thickness of the scattering material at area  $dA$ ,  
measured along the inward normal to  $dA$ ,

$i$  = the identity index of the material of which  $dA$   
is a part.

For a spectrum of source particle energies the energy integrated flux,  
 $\Phi_{\alpha S}(E_{\alpha S})$ , may be obtained by an integration similar to that of Equations  
(7) and (8), as

$$\Phi_{\alpha S}(E_{\alpha S}) = \int_0^{\infty} \phi_{\alpha S}(E_{\alpha S}) dE_0 \quad (14)$$

The flux term in the integrand of Equation (13) may be defined according to  
albedo theory as<sup>(2,4)</sup>

$$\phi_{\alpha S}(E_{\alpha S}) = \phi_0(E_0, r_1) \cdot \frac{\cos \theta_0 \cdot dA \cdot \alpha(E_0, \theta_0, \theta, \varphi, t; i)}{r_2^2}, \quad (15)$$

where

$\alpha(E_0, \theta_0, \theta, \varphi, t; i)$  = the angular differential number current  
albedo with respect to the noted argu-  
ments (defined for Equation (13))<sup>(2,4)</sup>,

$\phi_0(E_0, r_1)$  = number flux incident on area  $dA$ ,  
=  $S(E_0) \cdot G(r_1)$ , c.f. Equation (11).

The assumption underlying the use of the albedo technique for complex geo-  
metry analysis is that the scattered radiation particles emerge from the  
scattering medium surface at a point close to their point of entry. This  
assumption is generally justified<sup>(2)</sup>, eg. the separation distance between

entry and exit for one-half of all escaping gamma photons has been found to be less than one mean-free-path (for incident energy  $E_0$ ). Photon scattering from very thin or laterally small structures of volume  $V$ , may be alternately predicted by the single-scattering approximation method<sup>(5)</sup>, from the relationship

$$\phi_{\alpha ss} = \int_{\text{Volume}, V} \phi_0(E_0, r_1) \cdot \frac{N_e \cdot \sigma_{KN}(E_0, \theta_s) dV}{r_2^2} \quad (16)$$

where

$N_e$  = the scattering material electron density per cubic centimeter,

$\sigma_{KN}(E_0, \theta_s)$  = the Klein-Nishina angular-energy intensity distribution function<sup>(2)</sup>, for photons of energy  $E_0$  and scattering angle  $\theta_s$ ,

$\theta_s$  = the angle between the primary and scattered photon directions.

Equation (15) may be solved if values for the number albedo are known. The albedo may be determined by either a laboratory experiment or a Monte Carlo treatment. For gamma photons, recently developed modification of the moments method has been reported as a potential source of albedo data<sup>(6)</sup>. In the present work, experimental albedo data<sup>(7,8)</sup>, and empirical relationships in accord with both experimental and Monte Carlo results<sup>(2,4,9,10)</sup>, were used for gamma photons. A similar approach is proposed for the case of fast-neutrons.

Since weight is the product of volume and density, the weight optimization of an axially symmetric shadow shield of specified composition may be considered as an optimization of shield thickness,  $L_{\min}$ , such that



$\phi_D(E_D)_{\gamma, n} \leq C$ , where  $C$  is a specified criterion, eg. 10 particles/cm<sup>2</sup>-sec. The optimum, or minimum weight of a right-cylindrical shield of radius  $R$ , may be obtained as

$$W_{\min} = \pi R^2 l_{\min} \cdot \rho, \quad (17)$$

$$= \pi R^2 \sum_{i=1}^m l_{i\min} \cdot \rho_i, \quad (18)$$

where

$\rho_i$  = the density of shield material  $i$ ,

$\rho$  = the weighted density of the shield,

= the shield material actual density if  $m = 1$ .

The total number flux reaching the detector for the case of a polyenergetic source, is obtained from Equation (2) doubly integrated over primary and secondary energies, as

$$\begin{aligned} \Phi_D = \int_{E_D} \Phi_D(E_D)_{\gamma, n} dE_D &= \int_{E_O, E_\alpha} \phi_\alpha(E_\alpha)_{\gamma, n} dE_O dE_\alpha + \int_{E_O, E_a} \phi_a(E_O; E_a)_{\gamma} dE_O dE_\alpha + \\ &+ \int_{E_O, E_a} \phi_a(E_O; E_a)_n dE_O dE_\alpha \end{aligned} \quad (19)$$

where the subscripts  $\gamma$  and  $n$  denote gamma photons and fast neutrons. The use of the albedo and build-up factor concepts is tantamount to an integration over  $E_\alpha$  and  $E_a$ , respectively.

Equation (19) may be further redefined as

$$F = \int_{E_O, E_a} \phi_a(E_O; E_a)_{\gamma} dE_O dE_a + \int_{E_O, E_a} \phi_a(E_O; E_a)_n dE_O dE_a, \quad (20)$$

where

$$F = \int_{E_D} \phi_D(E_D) \gamma' n dE_D \int_{E_O, E_\alpha} \phi_\alpha(E_\alpha) \gamma' n dE_O dE_\alpha \quad (21)$$

$$= C - \int_{E_O, E_\alpha} \phi_\alpha(E_\alpha) \gamma' n dE_O dE_\alpha \quad (22)$$

The flux terms in Equation (20) may be obtained from Equations (10) and (13) and  $L_{\min}$  obtained by an iterative solution. For example, for a single material shield exposed to a monoenergetic source of neutrons and photons, Equation (20) reduces to

$$F = \phi_O(E_O)_\gamma B(E_O)_\gamma e^{-\mu(E_O)_\gamma L} + \phi_O(E_O)_n B(E_O)_n e^{-\mu(E_O)_n L}, \quad (23)$$

The foregoing theoretical discussion has presumed a knowledge of gamma photon and fast neutron interaction phenomena. Such phenomena and the relevant interaction physics are summarily reviewed in the Appendix. In addition, a familiarity with the solution of radiation transport problems by means of the Monte Carlo method is presumed; the reader is referred to the references in this regard<sup>(11,12)</sup>.

The second term in the right-side of Equation (20) is defined by Equation (2). It includes the shield originating neutron reaction product flux  $\phi_{aR}(E_{aR})$ , as yet not discussed in any detail. Although the flux  $\phi_{aR}(E_{aR})$  reaching the detector, may be predicted by means of either a laboratory experiment or a Monte Carlo code evaluation, it may be estimated for the case of reaction product gamma photons such as result from inelastic scatters or absorptions in an axially symmetric shadow shield, as

$$\phi_{aR}(E_{aR}) = \int_0^L g \cdot G(r_\ell) \cdot \Sigma_\gamma(E_O) \cdot \phi_O(E_O)_n \cdot (1 - e^{-\lambda \tau}) \cdot e^{-\Sigma_{Tot}(E_O) \ell} \cdot e^{-\mu(E_{aR})(L-\ell)} d\ell, \quad (24)$$

where

$g$  = the cross-section area of the axially symmetric shadow shield,

- $= \pi R^2$ , for a cylindrical shield,
- $\ell$  = the distance from the shield face at the source to the differential volume  $g.d\ell$ ,
- $G(r_\ell)$  = the geometry factor for distance  $r_\ell$ , c.f. Equation (11),
- $r_\ell$  = the distance from the differential volume  $g.d\ell$  to the detector,
- $\Sigma_\gamma(E_O)$  = the linear attenuation coefficient of the shield material for fast-neutrons of energy  $E_O$ , for production of gamma photons,
- $\Sigma_{Tot}(E_O)$  = the total linear attenuation coefficient of the shield material for fast-neutrons of energy  $E_O$ ,
- $\phi_O(E_O)_n$  = the shield normally and parallel incident flux of fast neutrons of energy  $E_O$ ,
- =  $\phi_O(E_O, (r_O - r_\ell))_n$ , c.f. Equation (11),
- $\mu(E_{aR})$  = the total linear attenuation coefficient of the shield material for reaction product gamma photons of energy  $E_{aR}$ ,
- $\lambda$  = the radioactive decay constant of the reaction-produced or compound nucleus,
- $\tau$  = the duration of exposure to the neutron flux,

For inelastic scattering the decay constant in Equation (24) is relatively large and thus

$$1 - e^{-\lambda\tau} \approx 1.0 \quad (25)$$

This is also true for activation where the product  $\lambda \cdot \tau$  is large.

A modified form of Equation (24), where  $g, l, r_l$  and the exponent  $\mu(E_{aR})(L-l)$  are replaced by  $dA, t, r_2$  and  $\mu(E_{aR}) \cdot t$  respectively, may be defined as

$$\phi_{aR}(E_{aR}) = \int_0^t dA \cdot G(r_2) \cdot \Sigma_y(E_0) \cdot \phi_0(E_0, r_1) (1 - e^{-\lambda\tau}) e^{-\Sigma_{Tot}(E_0)t} \cdot e^{-\mu(E_{aR})t} dt \quad (26)$$

to estimate the spacecraft structure reaction product 'albedo',  $\alpha_R$  for prediction of fluxes,  $\phi_{aR}(E_{aR})$ . This albedo, valid for normal incidence and emergence, may be substituted in Equation (29), to estimate the angular differential albedo. Primary and secondary energy integrations of Equations (24) and (26) are as defined for Equation (20).

The shadow shield as a secondary source of both photons and neutrons, ie. scattered and reaction product radiation, has been discussed. Scattering to the detector may be accounted for either by the use of the build-up factor concept or a Monte Carlo analysis and reaction product radiation intensity may be predicted by the use of Equation (24) or a Monte Carlo analysis. In addition to being a second order source, the shield may also be considered as third order source, ie. primary radiation interacting in the shield may produce secondary radiation which in turn interacts in the spacecraft structure to yield a third order flux at the detector.

The detected flux resulting from interactions in the spacecraft structure may be predicted in accord with either Equations (15), (16) or (26) and discussions thereto, providing the shield-originating flux  $\phi_0(E_{aR}, r_{1 \text{ shield}}) = \phi_0(E_{aR}, r_{1s})$ , is known and substituted for  $\phi_0(E_0, r_1)$ . It may be estimated

for right-cylindrical shadow shield axially perpendicular emission as,

$$\phi_0(E_{aR}, r_{1s}) = \int_0^L f(R, r_{1s}, E_{aR}) \cdot \Sigma_y(E_0) \cdot \phi_0(E_0) \cdot (1 - e^{-\lambda \tau}) \cdot e^{-\Sigma_{Tot}(E_0) \ell} d\ell, \quad (27)$$

where the function  $f(R, r_{1s}, E_{aR})$ , valid for  $\ell \ll r_{1s}$ , takes the shield self-absorption into account. This function is defined for a cylinder as

$$f(R, r_{1s}, E_{aR}) = \frac{g}{2\pi} \int_0^{\sin^{-1} \frac{R}{r_{1s}}} d\beta \int_{y_1}^{y_2} \frac{e^{-\mu(E_{aR})(y-y_1)}}{y} dy, \quad (28)$$

where

$$y_1 = r_{1s} \cos \beta - R \cos \psi,$$

$$y_2 = r_{1s} \cos \beta + R \cos \psi,$$

$$\psi = \pi - \sin^{-1} \left( \frac{r_{1s} \sin \beta}{R} \right),$$

$$y = \text{integration variable; a distance,}$$

$$\beta = \text{integration variable, an angle,}$$

$$r_{1s} = \text{the shield-to-spacecraft 'area dA' distance; analogous to } r_1.$$

For reasons of clarity the fluxes discussed in this report section are schematically summarized in Figure 3.

### 2.3. Code Logic

During the present report period ---Code SØSC --- a spacecraft shield optimization study code was designed in the FORTRAN-IV compiler language for the NASA-GSFC IBM-360/91 digital computer. The three major component sub-codes which make up SØSC: XEST, NUGAM1 and ALB, have been developed, debugged and are provisionally operational. Preliminary development of codes XEST and ALB was carried out on a CDC-6600 digital computer, accessed from the NUS Corporation CDC-Marc II high-speed terminal facility.

Preliminary data and resulting observation obtained with the SØSC component codes are given in Section 2.4. Code SØSC consists of a main controlling program --- MAIN, a shield thickness prediction program --- XEST, a complex geometry scatter flux program --- ALB, and a Monte Carlo build-up factor and albedo calculating program --- NUGAM1. Development work on these programs has focussed on gamma photon transport as noted in Section 1 of this report. Neutron transport has been evaluated according to 'removal' theory<sup>(2,13)</sup>.

MAIN executes input and final output operation. Details of the input-output are omitted from this report since they are still subject to some change. The main programs calls ALB to determine F for Equation (20). It calls XEST to estimate an approximate thickness value,  $L_{min_e}$ , for Equation (20). NUGAM1 is called to determine build-up factors corresponding to the estimated value of  $L_{min_e}$ . Using the thus determined values of F and the build-up factors, the code solves Equation (18) for the optimum thickness  $L_{min}$  by iteration. It will optionally recall NUGAM1 to determine the deviation of the build-up factors for  $L_{min}$  from those for  $L_{min_e}$ . If this deviation exceeds a tolerance value the code will reiterate. Code SØSC logic is summarized in Figure 4.

Code ALB determines the angular-energy integrated flux scattered to the detector by the spacecraft complex structural components illuminated by primary source radiation. Code ALB consists of an albedo package and a generalized geometry package. In its present form the albedo package is coded for gamma photons because of the lack of fast neutron differential number albedo data. It is proposed that fast neutron data be generated by a proposed Monte Carlo code.

The albedo routines in code ALB determine the scattered energy integrated

flux  $\phi_{\alpha s}(E_{\alpha s})$  defined by Equation (13). The main calling program carries out the integration over primary source energies. The gamma photon number current albedos defined by Equation (15) were obtained from the relationship

$$\alpha(E_o, \theta_o, \theta, \varphi, t; i) = \alpha(E_o, 0, 0, 0, \infty; i) \cdot f(\theta_o) \cdot \cos\theta \cdot g(t) , \quad (29)$$

$$= \alpha(E_o; i) \cdot f(\theta_o) \cdot \cos\theta \cdot g(t) , \quad (30)$$

where

$\alpha(E_o; i)$  = the angular differential number current albedo for gamma photons perpendicularly incident ( $\theta_o=0$ ) and emergent ( $\theta=0$ ) from scattering material  $i$ , ie.  $180^\circ (= \theta_s)$  backscatter,

$g(t)$  = a function to account for reduced backscattering from a material of finite thickness  $t$ ,

$f(\theta_o)$  = a function to account for the albedo behaviour with change in  $\theta_o$ .

From reference (14), the azimuthal dependence may be defined in terms of  $\theta$ ,  $\theta_o$  and the total scattering angle  $\theta_s$ , as

$$\varphi = \cos^{-1} \left[ \frac{\cos\theta_s + \cos\theta_o \cos\theta}{\sin\theta \sin\theta_o} \right]$$

where

$\theta_s$  = the angle between the incident and emergent photon vectors, i. e., the scattering angle.

The present version of code ALB temporarily assumes (7,8,10)

$$f(\theta_o) = \cos\theta_o , \quad (31)$$

and<sup>(9)</sup>

$$g(t) = \alpha(E_o, t; i) / \alpha(E_o; i) , \quad (32)$$

$$= 1 - e^{-ct} , \quad (33)$$

where  $c$  is a constant such that  $g(t) = 0.99$ , for  $t = 2 \lambda(E_0)_i$ ;  $\lambda(E_0)$  is the mean-free-path in material  $i$  for photons of energy  $E_0$ . Code ALB uses scattering angle  $\theta_s$  to eliminate the albedo dependence on azimuth  $\phi$ , in accord with the method of reference (14).

For code preliminary runs experimentally measured values for the perpendicular number current albedo  $\alpha(E_0; i)$  were obtained from references (7, 8). For fast neutrons, Monte Carlo data from reference (10) was used for preliminary evaluations.

The generalized geometry routine for code ALB requires that the spacecraft structure be redefined as simple geometrical shapes, eg. cylinders, rectangular boxes, prisms, slabs, etc. These shapes allow the flat-sided cylindrical spacecraft body, boom-arms, antennae, science platforms, etc. to be accounted for. The theory and logic of the geometry code will be detailed in the final report to this contract.

Code NUGAM1 determines the angular energy transport of gamma photons in a finite cylindrical shield. It was derived from an existing source self-absorption code --- NUALGAM, developed for NASA-GSFC by NUS Corporation, and described in NUS-536<sup>(15)</sup>. It considers pair-production, Compton scattering and photoelectric interaction phenomena.

In code NUGAM1, the shield may be composed of a single material of simple or complex composition or stratifications ie. "discs", of simple or complex composition, including vacuum. The code is presently designed for either an axial point or plane parallel source but may be readily adapted to other distributions. Similarly, the code may be readily modified to allow the study of annular-cylindrical shields, rectangular slabs, etc.

Code NUGAM1 may be used to determine angular differential forward build-up and albedos for gamma photons. Preliminary studies with this code, which may be either called by code SØSC or used as a separate code,



have revealed that the forward build-up factor for the shadow shields is less than that to be expected for a large (semi-infinite) shield, in agreement with qualitative argument. This is summarily discussed in Section 2.4.

Code XEST determines the value of  $L_{\min}$  satisfying equation (20) and thus obtains  $W_{\min}$  of equation (17), or the  $\ell_{i\min}$  of equation (18). Although specifically designed for the purpose of shadow shield optimization it is coded for larger shields. Code XEST solves equation (20) by the technique of iteration. For the first iteration the code assumes a build-up factor of unity to determine  $L_{\min_e}^{(1)}$ . For the second iteration a Monte Carlo build-up factor based on  $L_{\min_e}^{(1)}$  and calculated by NUGAM1 is used to iterate  $L_{\min_e}^{(2)}$ . Iteration is arrested when

$$\left| (L_{\min_e}^{(h)} - L_{\min_e}^{(h-1)}) / L_{\min_e}^{(h)} \right| \leq \epsilon, \quad (34)$$

where

$\epsilon$  = preassigned tolerance,

$h$  = iteration number.

## 2.4 Discussion

Preliminary results obtained with the SØSC component codes are reviewed in this report section. They consist of shield thicknesses and weight evaluations for assumed typical SNAP-27 RTG source strengths and spectral distributions. Example results obtained for the scattering from spacecraft structural members are presented; and the importance of various factors discussed.

The calculations described in this section are based on a RTG gamma photon emission distribution similar to that of the Martin Cronus<sup>(16)</sup> (thermal loading of 4100 watts) normalized to a total emission of  $1 \times 10^9$   $\gamma$ /sec. The normalization factor has been discussed in Section 1. The RTG fast neutron

emission distribution was based on SNAP-27-1 reported data from reference (1); a source emission rate of  $5.7 \times 10^8$  n/sec was assumed. For both fast-neutrons and gamma photons, axial and axially perpendicular emission rates were taken as identical, although this is not true in fact. This assumption was necessitated by the lack of actual encased RTG source data. The assumed source emission spectrum is given in Table I for gamma photons and in Table II for fast neutrons.

The typical spacecraft for which the calculations were carried out is that of Figure 1, The Outer Planets Explorer. The dimensions of this spacecraft were obtained either directly or by scaling, from NASA-GSFC preliminary drawings. Figure 5 shows a schematic outline of this spacecraft for the discussions in this section.

Gamma photon cross-section data were taken from references (17) through (21). Neutron cross-section data were obtained from references (13) and (22).

The Table I source spectrum is that for a 3 year old  $\text{PuO}_2$  SNAP-27. Calculations in reference (16) indicate that the total gamma emission rate will increase by a factor of  $\sim 4$  over 18 years. Table III, reproduced from the reference, indicates that the energy groups 0.2 to 0.3, and 2.0 to 3.0 MeV are the most critical, eg. the 2.0 to 3.0 MeV group (2.62 MeV  $\text{ThC}''$ ) increases by a factor of more than 100 in the first 10 years. This age effect on shielding requirements was not studied during this report period because of lack of reliable source data.

The scattering of source gamma photons to the detector by aluminum boom tubing proximate to the source (or the detector) was investigated. The boom axis was assumed as perpendicularly bisecting a 16" long unit (1 $\gamma$ /sec)

source, for  $E_0 = 0.75$  MeV. The calculations assumed the boom as coming to within 10 cm of the source, although 25 cm is indicated by scaling the GSFC drawings. The calculations assumed a line source and a single scattering model for a boom tube volume of 0.79 cc/cm. The results of the calculations are shown in Figure 6 along with the calculation geometry. The detector-incident scattered flux for a single typical boom (boom (1,2) in Fig. (5)) is obtained from Figure 6 as  $\phi_{\alpha S}(E_\alpha) = 1.3 \times 10^{-11}$   $\gamma/\text{cm}^2\text{-sec}$ . Assuming boom (1,2) in Figure 5 as typical, where  $r_1$  ranges from 25 to 80 cm, ie. a length of 55 cm, the total scattered flux from 6 such booms (6 per side) and 4 RTG sources would be  $\sim 3 \times 10^{-10}$   $\gamma/\text{cm}^2\text{-sec}$ .

The use of the single scattering model as opposed to the albedo method for boom structure calculations, was investigated. A 1 cm length of aluminum boom was considered as located 100 cm from both a point source and a detector, with source and detector 141 cm apart. For  $E_0 = 0.75$ , a unit source (1  $\gamma/\text{sec}$ ) and a boom volume 0.79 cc/cm, the calculated fluxes were

$$\begin{aligned}\phi_{\alpha S}(E_\alpha) &= 3.6 \times 10^{-12}, \gamma/\text{cm}^2\text{-sec}, \\ \phi_{\alpha SS}(E_\alpha) &= 6.4 \times 10^{-12}, \gamma/\text{cm}^2\text{-sec}.\end{aligned}$$

The difference in these calculations diminishes if it is assumed in the case of the albedo result that photons penetrating the relatively thin (0.04") tube frontal wall may be backscattered from the tube interior wall surface ie, if the wall thickness is doubled for the calculation, then

$$\phi_{\alpha S}(E_\alpha) = 7.0 \times 10^{-12}, \gamma/\text{cm}^2\text{-sec}.$$

This last result is only slightly greater than  $\phi_{\alpha SS}(E_\alpha)$ . The conclusion may be drawn that the single scattering result is a reasonable and valid approximation.

A similar calculation for a large cylinder, in the physical position of the spacecraft cupula, was carried out for iron as the material, dimensions 20" x 38.5" x 0.5" (dia. x lt. x thickness) and incident energy  $E_0 = 0.75$  MeV. The calculated fluxes were

$$\phi_{\alpha s}(E_\alpha) = 2.4 \times 10^{-9} \text{ } \gamma/\text{cm}^2\text{-sec},$$

$$\phi_{\alpha ss}(E_\alpha) = 2.7 \times 10^{-9} \text{ } \gamma/\text{cm}^2\text{-sec}.$$

For aluminum and a thickness of 1 inch, the singly scattered flux was

$$\phi_{\alpha ss}(E_\alpha) = 1.8 \times 10^{-9} \text{ } \gamma/\text{cm}^2\text{-sec}.$$

Taking an actual cupula 'flat', A, in Fig. (5), with dimensions 13.2" x 25.5" (width x lt.) and an assumed aluminum thickness of 1", the albedo technique flux was determined as

$$\phi_{\alpha s}(E_\alpha) = 1.8 \times 10^{-10} \text{ } \gamma/\text{cm}^2\text{-sec}.$$

Since  $\phi_{\alpha s}(E_\alpha) \sim \phi_{\alpha ss}(E_\alpha)$ , the scattered and detector incident flux from the twelve cupula 'flats' would be  $\sim 2 \times 10^{-9}$ , which is in good agreement with the large cylinder approximations; this assumes no attenuation of the 'flat'-transmitted radiation.

The above calculations were based on a single RTG source of 1 photon/sec, and  $E_0 = 0.75$ . Taking the source as  $10^9 \text{ } \gamma/\text{sec}$ , the detected scattered flux would approximately equal the contract criterion,  $C \leq 10 \text{ particles/cm}^2\text{-sec}$ . However, recent calculations using the photon spectrum of Table I indicate

$$\phi_\alpha(E_\alpha) \approx 0.1, \text{ } \gamma/\text{cm}^2\text{-sec},$$

for the large iron cylinder model, and

$$\phi_\alpha(E_\alpha) \approx 0.15, \text{ } \gamma/\text{cm}^2\text{-sec},$$

for the flat aluminum surface,  $A_1$ . Although these values are less than the single energy calculated values, they indicate that spacecraft structure scattering may in some problems be significant relative to the criterion C. It is proposed to study this problem further in the remainder of the contract period. If this photon scattering is considered significant enough to require shielding then such shielding would be a minimum weight if designed to attenuate the scattered photons as opposed to the primaries. The scattered photon energies will generally be in the range, 0.15 to 0.5 MeV, and thus readily attenuated by a thin shield located at the detector.

The foregoing calculations were obtained with the SØSC component code, ALB. Figures (7) and (8) are sodium-iodide scintillation detector spectra reproduced from reference (7) which indicate the ratio of single to multiple scattering as a function of  $t$  and  $\theta_0$ , respectively, for graphite as the back-scattering material. The prominent peak in these spectra is the single scatter distribution.

Table IV gives example optimum results for shield thicknesses and weights as predicted by code XEST, for lithium-hydride, aluminum, iron and lead. The calculations assumed the source spectra of Tables I and II. Build-up factors of 1.05, 1.3 and 1.5 were used for both gamma photons and neutrons in these preliminary calculations. The choice of these values is discussed below. The calculations do not include reaction product radiation.

The preliminary photon number build-up factors used in XEST were obtained from the Monte Carlo code NUGAM1. A point source axially located 8 cm from the shield was used throughout. Investigations are now being carried out for radiation axially-parallel incident. Early determinations were based on  $\mu L \sim 2.0$  from which build-up factors of  $\sim 1.05$  resulted. Recent determinations have indicated that higher values are likely since, as Table IV

indicates,  $\mu L \sim 4$ . For  $E_o = 1.25$ , the NUGAM1 point source code version predicts build-up factors  $\sim 1.3$ , for  $\mu L \sim 4.0$ .

Examples of energy-integrated scatter photon angular distributions are presented in Figure 9. The angular categorization is referenced to the shield geometric center. The distributions were determined by the Monte Carlo subprogram: NUGAM1. The current code version determines the photon distribution to which the detector is specifically exposed, i.e., photons escaping from the shield sides are considered as not intercepting the detector.

Table V gives sample number build-up factors as determined by code NUGAM1 for the noted materials and photon energies. They are based on 10,000 source photons uniformly distributed in the source-shield solid angle subtended by the circular shield face. The build-up factors in this Table must be considered as high since they include some shield side escape i.e., the forward categorizing solid-angle had a half-angle of  $10^\circ$ .

Further progress with respect to the foregoing will be reported in the monthly progress reports and the contract final report.

### 3. WORK PROGRAM FOR SECOND TERM

Throughout the second and remaining term of this contract, the work program will be carried to completion. Code SØSC will be integrated, debugged and made operational on the NASA/GSFC IBM-360/91 digital computer. Code SØSC will be run to determine the optimum shield for the spacecraft example of Figure 1. The preparation of a detailed user's manual and code description will complete the work scope outlined under Tasks I and II of this contract.

The design of a suitable and appropriate laboratory experiment will be carried out to verify the code SØSC shielding predictions. This result of this design will be incorporated into the code user/description manual, which will represent the contract final report.

## REFERENCES

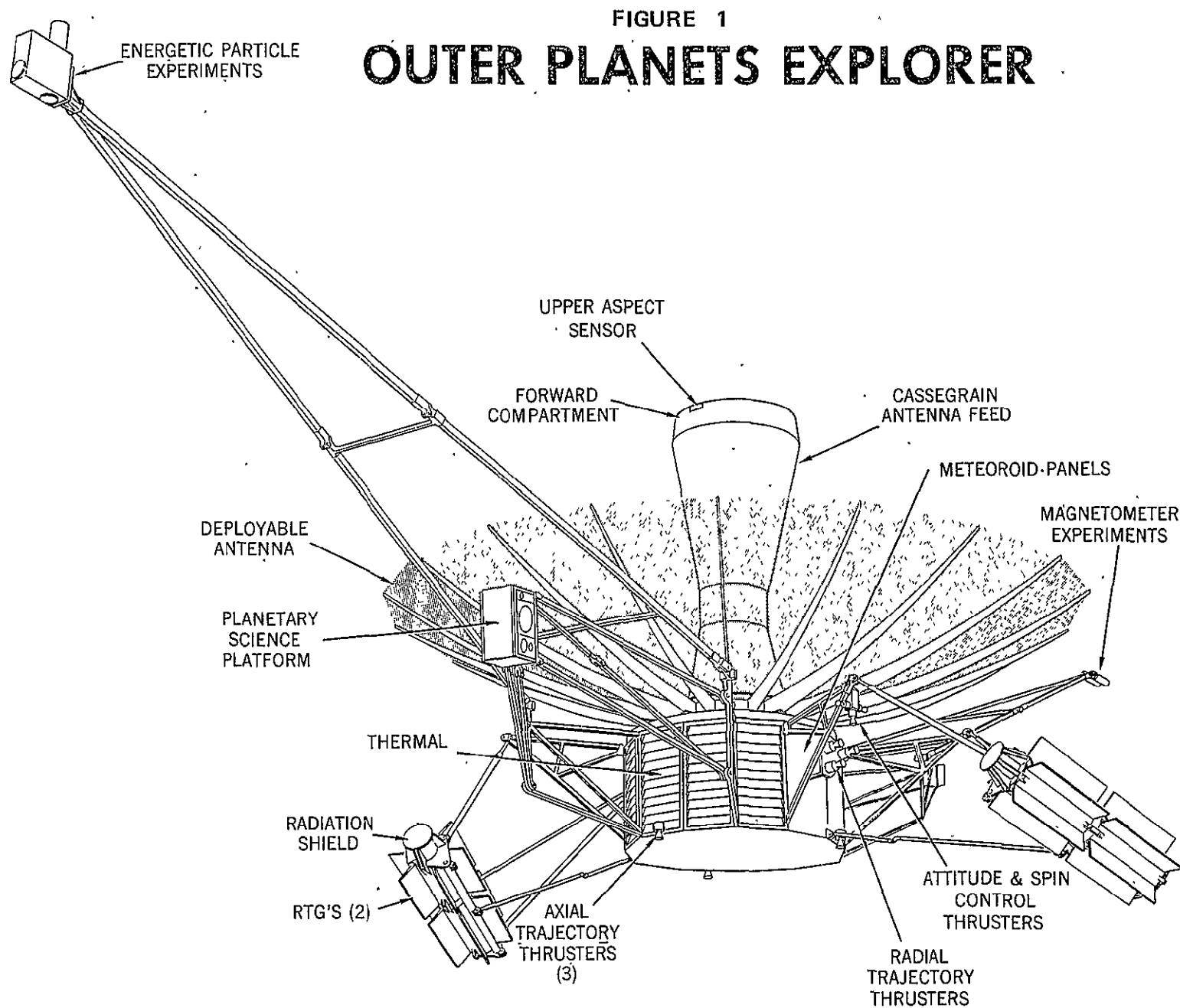
1. ANDERSON, M. E., and NEFF, R. A., "Neutron Emission Rates and Energy Spectra of Two Pu<sup>238</sup> Power Sources", Nuclear Applications and Technology, 7, 62-65 (1969).
2. JAEGER, R. G., Editor-in Chief, "Engineering Compendium on Radiation Shielding", Vol. I: Shielding Fundamentals and Methods, Springer-Verlag, New York, Inc. (1968).
3. TRUBEY, D. K., "A Survey of Empirical Functions Used to Fit Gamma Ray Build-up Factors", ORNL-RSIC-10 (1966).
4. SELPH, W. E., "Neutron and Gamma-Ray Albedos", ORNL-RSIC-21 (1968).
5. ROCKWELL III, THEODORE, Editor, "Reactor Shielding Design Manual", TID-7004, p. 317 (1956).
6. SMITH, C. V. and SCOFIELD, N. E., "The Moments Method Used to Determine the Energy Albedo of Gamma Rays from Cesium-137 Impinging on Aluminum and Iron Barriers", USNRDL-TR-67-120, U. S. Naval Radiological Defense Laboratory, (September 1967).
7. STEYN, J. J., "Backscatter of Normally Incident Gamma Photons From Semi-Infinite Media of Varying Atomic Number", Ph.D. Thesis, Univ. of Toronto (1965).
8. STEYN, J. J. and ANDREWS, D. G., "Experimental Differential Number, Energy and Exposure Albedos for Semi-Infinite Media, for Normally Incident Gamma Photons", Nucl. Sci. Eng., 27, 318 (1967).
9. BULATOV, B. P. and GARUSOV, E. A., "Co<sup>60</sup> and Au<sup>198</sup> Gamma Ray Albedos of Various Materials", J. Nucl. Energy, Part A: Reactor Science, 11, 159 (1960).
10. FRENCH, R. L. and WELLS, M. B., "An Angle-Dependent Albedo for Fast-Neutron-Reflection Calculations", Nucl. Sci. Eng., 19, 441-448 (1964).
11. CASHWELL, E. D., and EVERETT, C. J., "Monte Carlo Method For Random Walk Problems", Pergamon Press (1959).



12. SHREIDER, YU A. (Editor), "The Monte Carlo Method", Pergamon Press (1966).
13. AVERY, A. F., et al., "Methods of Calculation for Use in the Design of Shields for Power Reactors", AERE-R-3216 (1960).
14. SHOEMAKER, N. F. and HUDDLESTON, C. M., "Economy of Experiment in Dose Albedo", Nucl. Sci. Eng., 18, 113-115 (1964).
15. STEYN, J. J. and STRAHL, J. T., "NUALGAM - A Monte Carlo Code to Predict the Angular Energy Escape of Gamma Photons from Cylindrical Sources", NUS-536 (1969).
16. MILLER, C. G. and TRUSCELLO, V. C., "Compatibility Considerations Between Radioisotope Thermoelectric Generators and Scientific Experiments on Spacecraft", Jet Propulsion Laboratory, Engineering Memo: 342-83 (1969).
17. WHITE-GRODSTEIN, G., "X-Ray Attenuation Coefficients from 10 keV to 100 MeV", NBS Circular 583 (1957).
18. MCGINNIES, R. T., "X-Ray Attenuation Coefficients from 10 keV to 100 MeV", Supplement to NBS Circular 583 (1959).
19. HUBBELL, J. H. and BERGER, M. J., "Photon Attenuation and Energy Absorption Coefficients Tabulations and Discussion", NBS report 8681 (1966).
20. STORM, E., GILBERT, E., and ISRAEL, H., "Gamma Ray Absorption Coefficients For Elements 1 to 100 Derived from Theoretical Values of NBS", LASL-2237 (1958).
21. HUBBELL, J. H., "Photon Cross Sections, Attenuation Coefficients, and Energy Absorption Coefficients From 10 keV to 100 GeV", NSRDS-NBS 29, (1969).
22. GOLDBERG, M. D., et al., "Neutron Cross Sections", BNL-325, Second Edition, Supplement Number 2.
23. EVANS, R. D., "The Atomic Nucleus", McGraw-Hill Book Co., Inc., (1955)
24. FANO, U., SPENCER, L. V., and BERGER, M. J., "Handbuch der Physik", XXXVIII/2, 660, (1959)

25. HEITLER, W., "The Quantum Theory of Radiation", Third Edition, Oxford University Press, (1960)
26. COMPTON, A. H., and ALLISON, S. K., "X-Rays in Theory and Experiment", D. Van Nostrand Co., Second Edition, (1963)
27. FANO, U., Nucleonics, "Gamma-Ray Attenuation", 11, 8-12, 9, & 55-61, (1953)
28. SEGRÉ, E., "Nuclei & Particles", Benjamin Publishing Company, (1964)
29. BLATT, J. M., and WEISSKOPF, V. F., "Theoretical Nuclear Physics", John Wiley & Sons, (1958)

## FIGURES



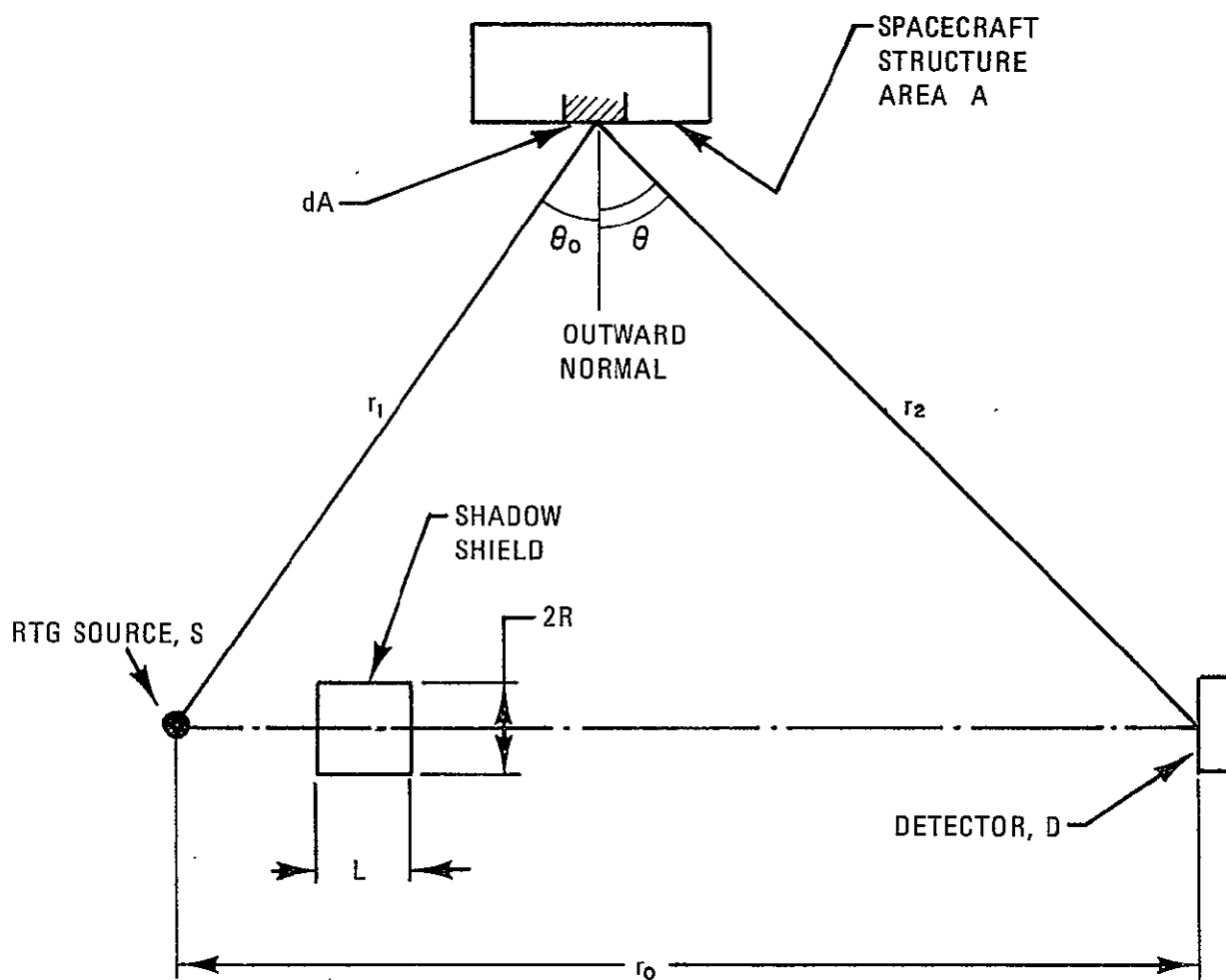
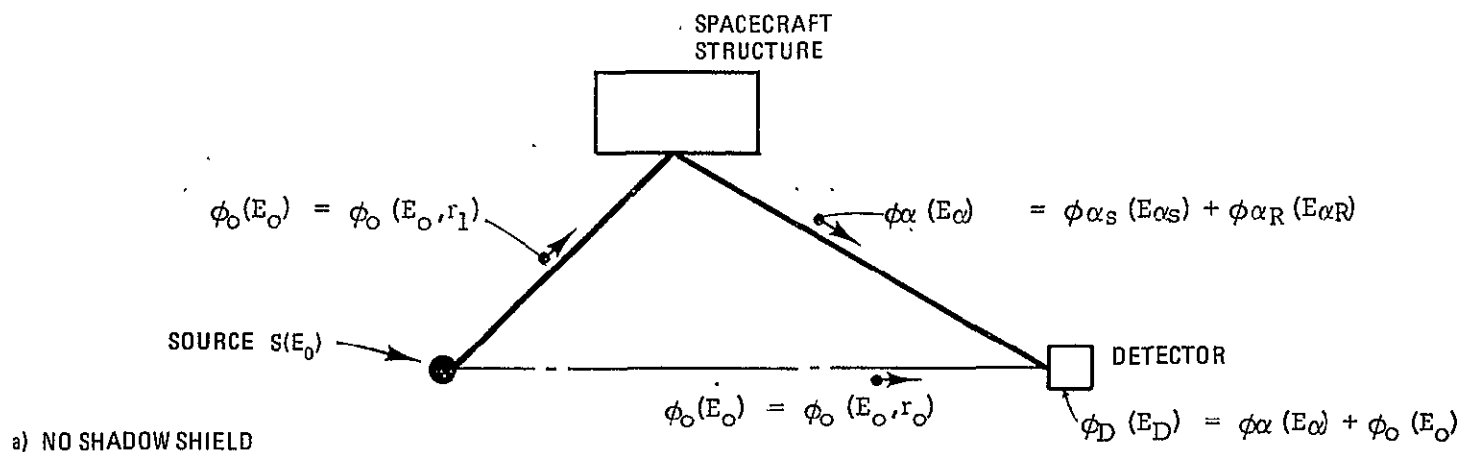


FIGURE 2  
SCHEMATIC DRAWING OF SPACECRAFT SHOWING  
RTG SOURCE SHIELD, AND DETECTOR ARRANGEMENT



b) WITH SHADOW SHIELD

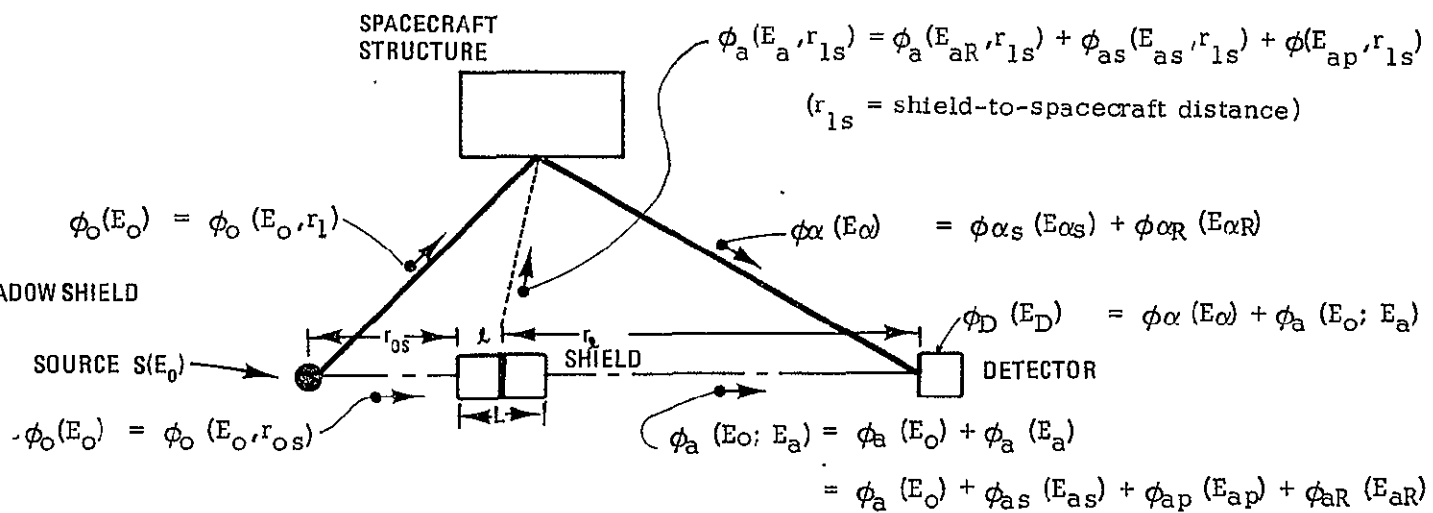


FIGURE 3

## SCHEMATIC DEFINITION OF GAMMA PHOTON AND NEUTRON FLUXES

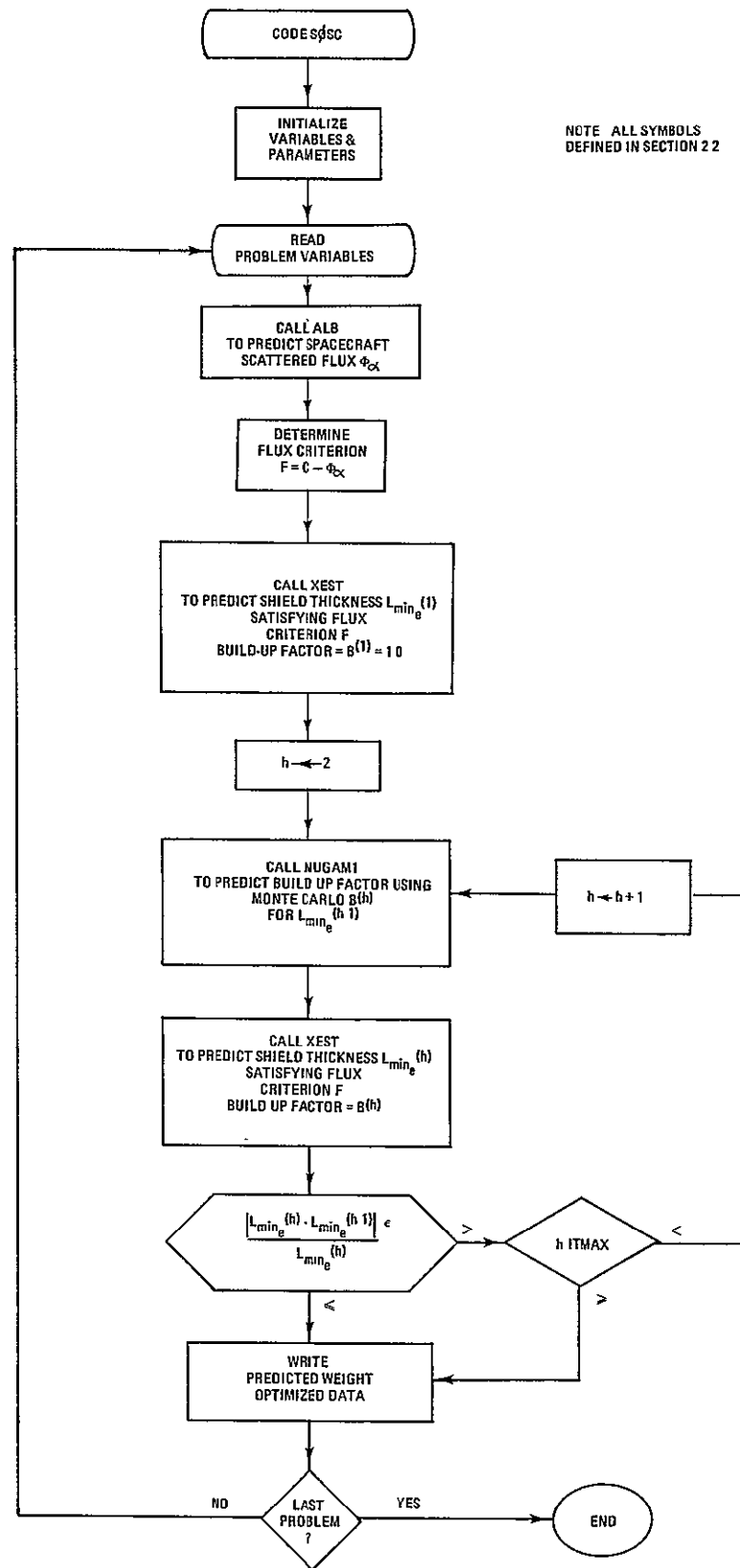


FIGURE 4  
CODE SPSJC LOGIC

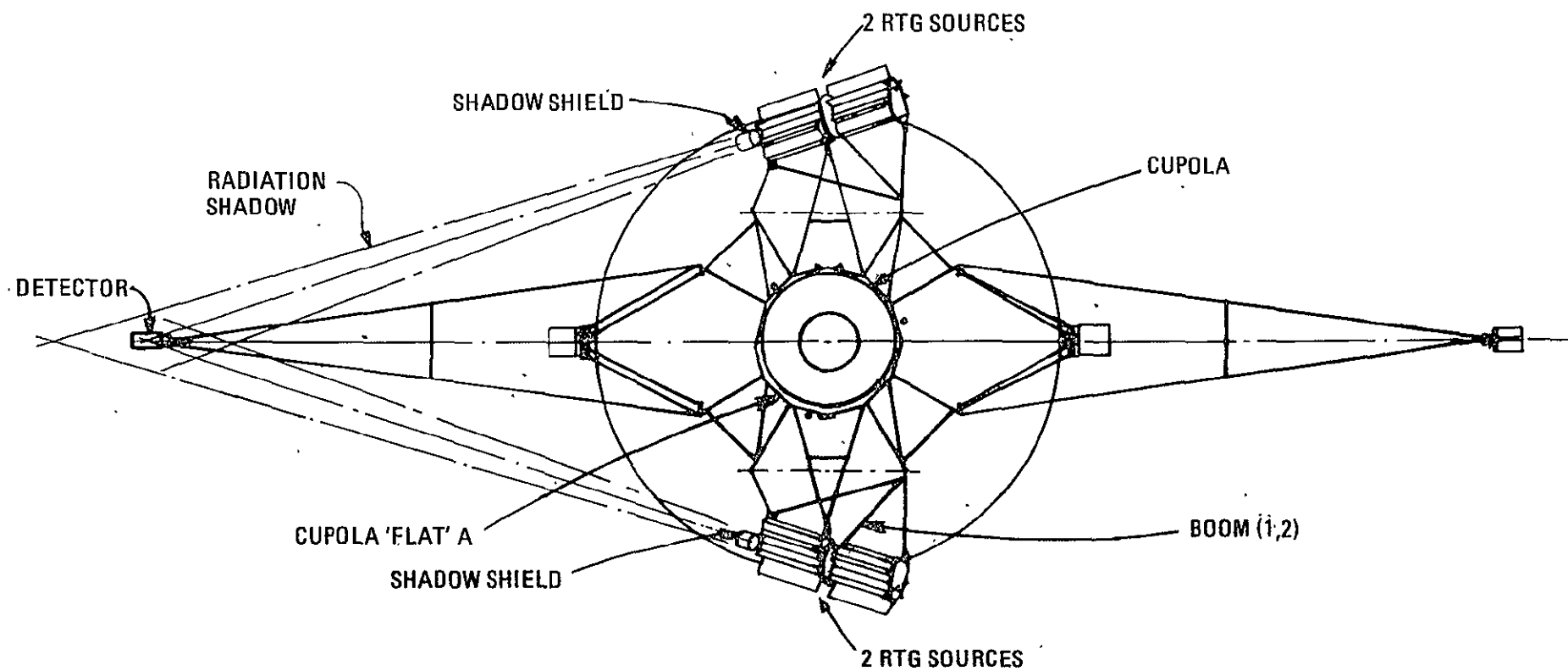


FIGURE 5  
SCHEMATIC DRAWING OF SPACECRAFT  
SHOWING SPECIFIC STRUCTURAL MEMBERS



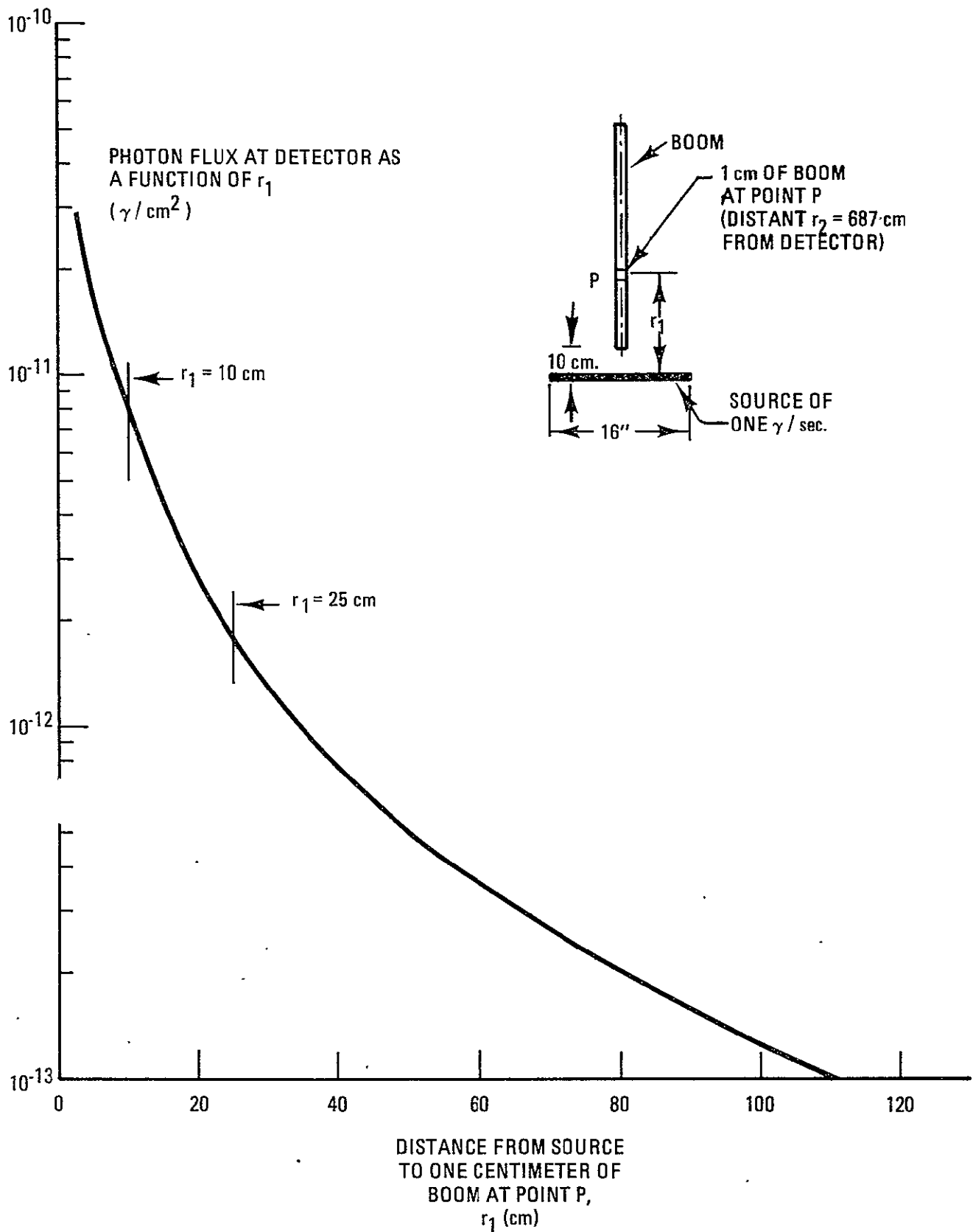


FIGURE 6  
BOOM SCATTER INTENSITY AS A FUNCTION  
OF SOURCE-TO-BOOM DISTANCE

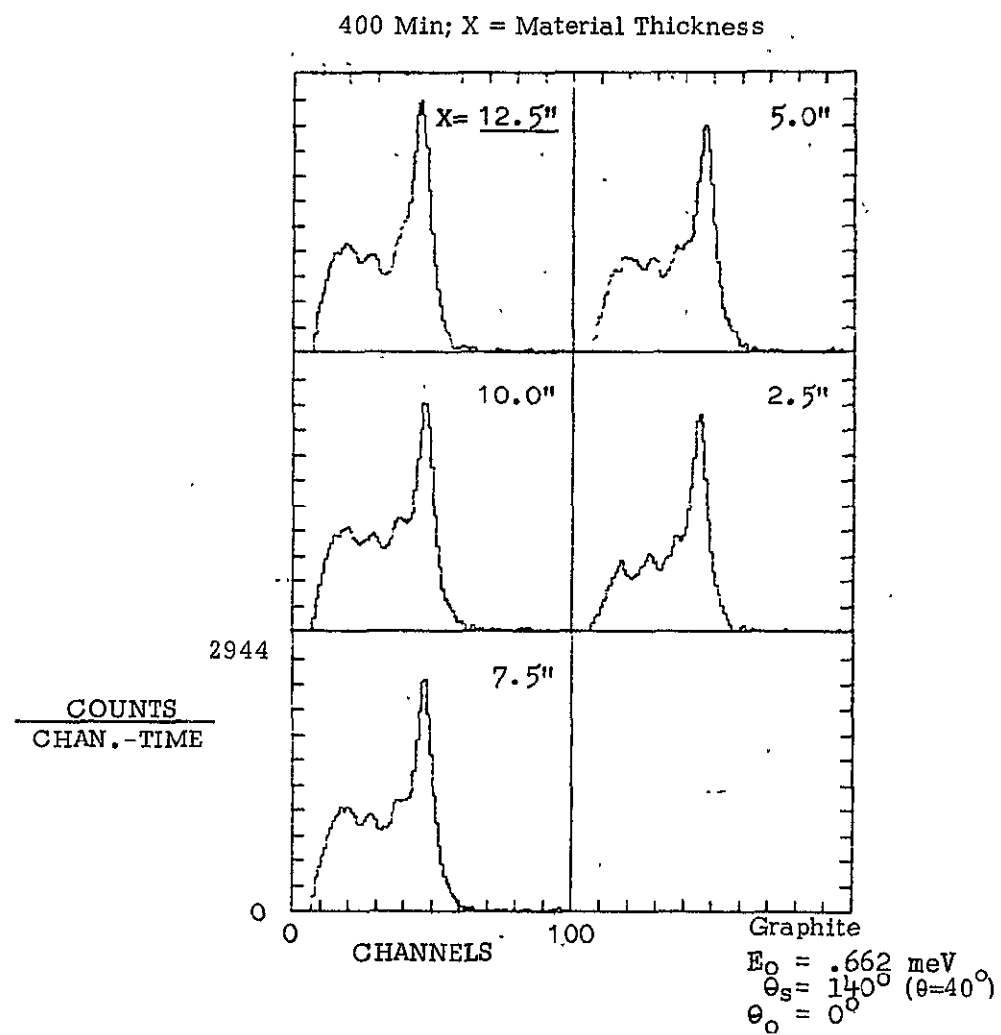
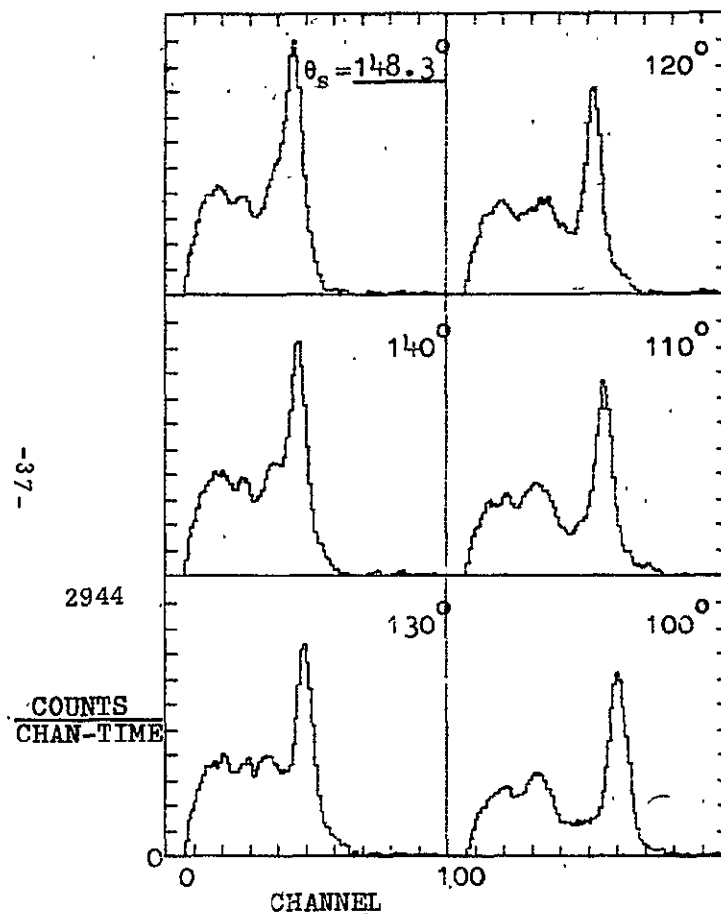


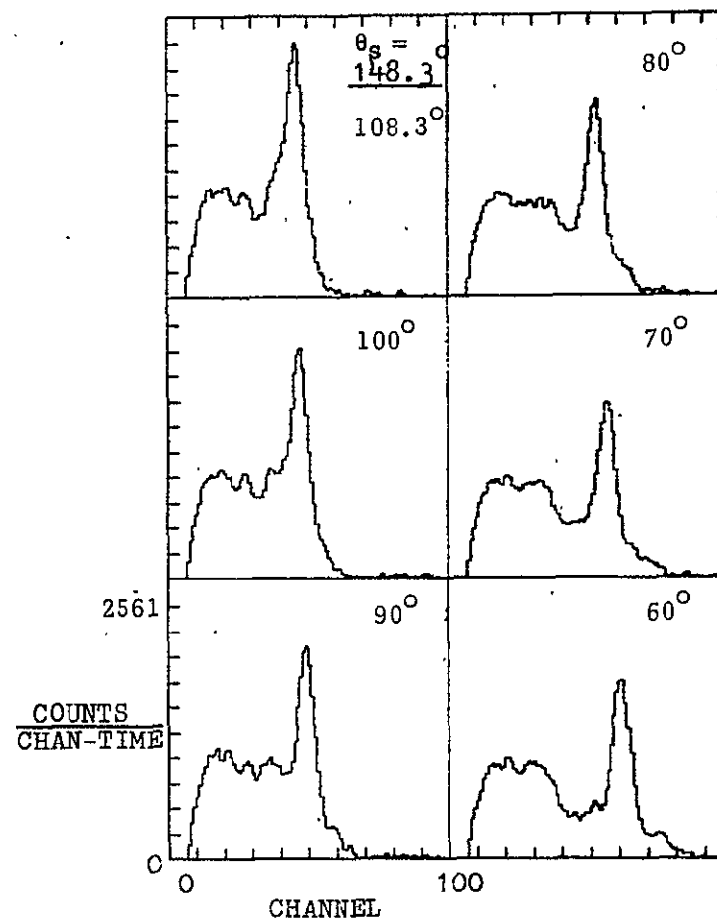
FIGURE 7  
 NaI(Tl) Scintillation Spectra Showing  
 Gamma Photon Backscatter Distribution as a  
 Function of Scattering Material Thickness

$\text{Cs}^{137}$ ; Graphite  
400 Min;  $\theta_s = 80 - (\theta_o + \theta)$



8 (a) Perpendicular Incidence:  
Spectral Distribution as a Function  
of Scatter Angle  $\theta_s$  for  $E_o = 0.662$  MeV  
and  $\theta_o = 0^\circ$

$\text{Cs}^{137}$ ; Graphite  
400 Min;  $\theta_s = 180 - (\theta_o + \theta)$



8 (b) Slant Incidence:  
Spectral Distribution as a Function  
of Scatter Angle  $\theta_s$  for  $E_o = 0.662$  MeV  
and  $\theta_o = 40^\circ$

FIGURE 8

NaI(Tl) Scintillation Spectra Showing  
Gamma Photon Scatter Distribution as a  
Function of Incident-Angle,  $\theta_o$

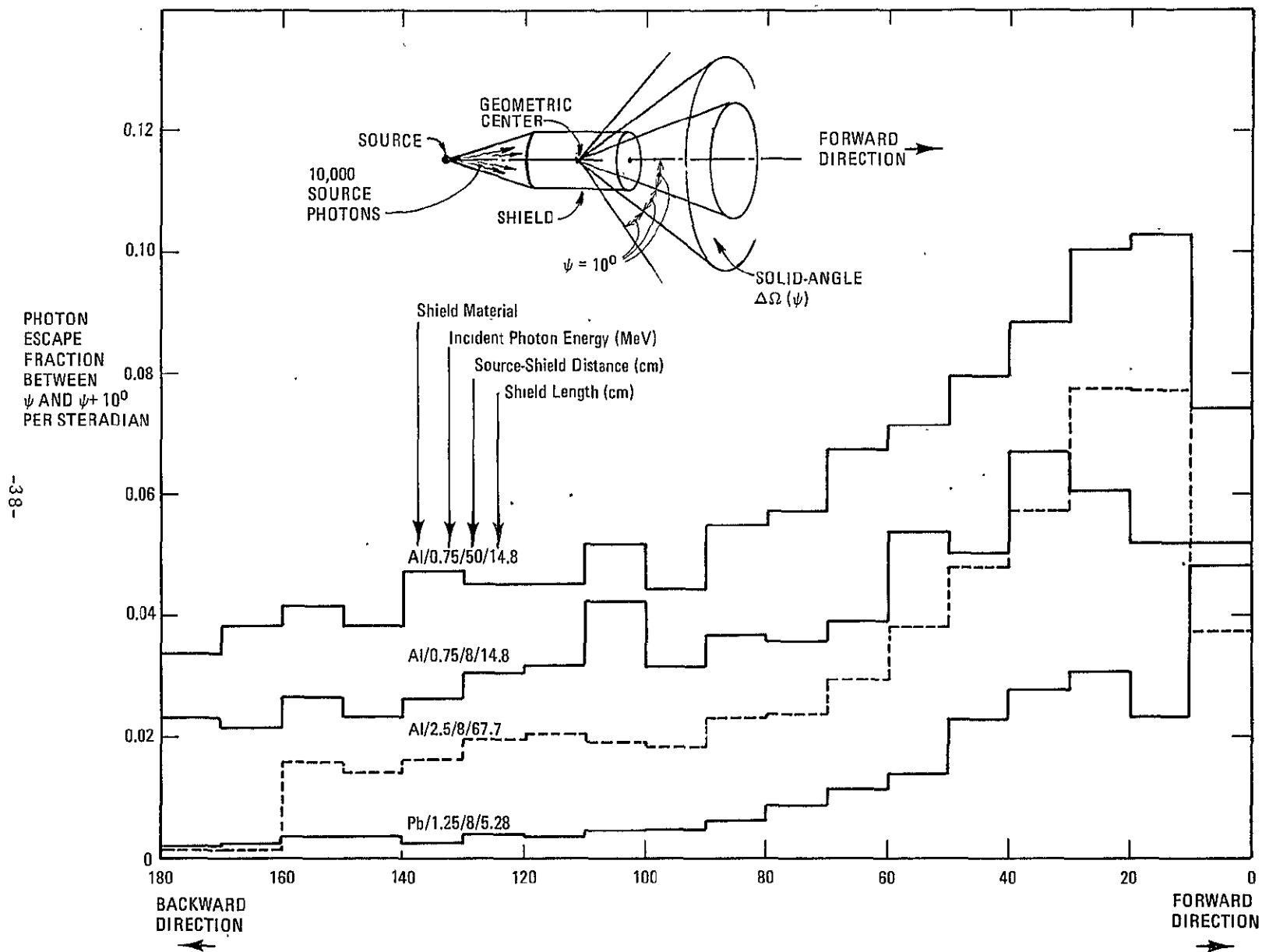


FIGURE 9  
ENERGY-INTEGRATED ANGULAR DISTRIBUTION  
OF SHIELD SCATTERED PHOTONS

TABLES I to V

TABLE I

Assumed SNAP-27 Gamma Photon Emission Spectrum  
Based On Martin Cronus Data<sup>(16)</sup>

Energy Interval (MeV)	Assumed Energy (MeV)	Photon Emission Rate ( $\gamma$ /MeV-sec)
0.044 - 0.2	0.15	$6.54 \times 10^7$
0.2 - 0.3	0.24	$6.87 \times 10^7$
0.3 - 0.4	0.311	$7.88 \times 10^7$
0.4 - 0.5	0.414	$7.86 \times 10^7$
0.5 - 0.6	0.583	$8.03 \times 10^7$
0.6 - 0.7	0.650	$7.33 \times 10^7$
0.7 - 0.8	0.766	$2.26 \times 10^8$
0.8 - 0.9	0.851	$1.40 \times 10^8$
0.9 - 1.0	1.00	$6.65 \times 10^6$
1.0 - 1.2	1.10	$1.87 \times 10^7$
1.2 - 1.4	1.40	$1.73 \times 10^7$
1.4 - 1.6	1.59	$7.71 \times 10^6$
1.6 - 1.8	1.63	$1.63 \times 10^7$
1.8 - 2.0	1.90	$1.54 \times 10^7$
2.0 - 3.0	2.61	$1.07 \times 10^8$
3.0 - 4.0	3.50	$3.03 \times 10^5$
4.0 - 5.0	4.50	$9.10 \times 10^3$
5.0 - 6.0	5.50	$3.01 \times 10^4$

TABLE II

SNAP-27-1 Fast Neutron Emission Spectrum<sup>(1)</sup>

Energy Interval (MeV)	Neutron Emission Rate (n/MeV-sec)
0 - 1.0	$5.06 \times 10^7$
1.0 - 3.0	$4.16 \times 10^7$
3.0 - 4.0	$1.79 \times 10^7$
4.0 - 5.0	$3.56 \times 10^6$
5.0 - 6.0	$1.90 \times 10^6$
6.0 - 8.0	$4.50 \times 10^5$
8.0 - 10.0	$1.14 \times 10^5$

Energy Integrated Emission Rate =  $5.7 \times 10^7$  n/sec.

TABLE III

Reproduced from Reference (16)

Gamma spectra, photons/cm<sup>2</sup>-sec for RTG at various times  
after plutonium separation (Normalized to 1.0 for  
energy interval 0.5-1.0 MeV at 18 years)

Energy (MeV)	0 year	1 year	5 year	10 year	18 year
0.04 - 0.5	0.12	0.16	0.56	0.90	1.0
0.5 - 1.0	0.23	0.25	0.30	0.33	0.35
1.0 - 2	0.096	0.096	0.096	0.096	0.096
2 - 3	0.003	0.018	0.18	0.32	0.37
3 - 5	0.0003	0.0003	0.0003	0.0003	0.0003
5 - 7	0.00003	0.00003	0.00003	0.00003	0.00003



TABLE IV

Optimized Shield Thicknesses And Weights  
Based On Provisional Build-Up Factor Data\*

Shield Material	density, $\rho$ (g/cc)	B = 1.05		B = 1.3		B = 1.5	
		length, L (cm)	weight, W (kg)	length, L (cm)	weight, W (kg)	length, L (cm)	weight, W (kg)
lithium- hydride (Li H)	0.82	56.28	1.46	60.90	1.58	64.1	1.66
aluminum (Al)	2.699	18.3	1.57	19.8	1.69	20.7	1.77
iron (Fe)	7.87	7.44	1.85	8.10	2.02	8.54	2.13
lead (Pb)	11.35	5.80	2.08	6.54	2.35	7.08	2.54

\*Right-Cylindrical Shield of Radius 1.25 inches.

TABLE V

Provisional Build-Up Factors Predicted By Code NUGAM1

Shield Material	length, L (cm)	Photon Energy, $E_0$ (MeV)	Number of Mean-Free Paths, $\mu(E_0)L$	Flux at Detector ( $\gamma/\text{cm}^2$ )		Build-Up Factor, B
				Unscattered $\phi_a(E_0)$	Scattered $\phi_a(E_a)$	
LiH	29.1	1.25	1.37	.0450	.000615	1.025
LiH	29.1	0.25	2.7	.0115	.00121	1.05
Al	67.7	2.5	7.05	.000153	.000868	6.67
Al	27.5	1.25	4.07	.00301	.00102	1.34
Al	14.8	0.75	2.81	.00112	.0112	1.10
Fe	4.89	0.75	2.64	.00124	.0126	1.10
Pb	5.28	1.25	3.46	.00104	.00554	1.188

APPENDIX  
INTERACTION PHYSICS REVIEW

## APPENDIX

### INTERACTION PHYSICS REVIEW

#### I GAMMA PHOTON INTERACTION PHENOMENA

In their passage through a medium, photons interact with the electrons and nuclei of atoms in their path. These phenomena form the basis both for their detection and for the deposition of their energy. A discussion of the kind and effect of these interactions as they pertain to the present work is given in this report section <sup>(23-27)</sup>.

There are four kinds of basic gamma photon interaction processes <sup>(27)</sup>, of which only two are relevant in the present work, namely:

- a) interaction with atomic electrons,
- b) interaction with the electric field surrounding nuclei or electrons.

The effect of (a) may be either scattering or absorption; the latter is the Photoelectric Effect. The scattering may be either one of the two types:

- 1. Compton inelastic scattering (incoherent), or
- 2. Rayleigh elastic scattering (coherent).

The effect of (b) is the disappearance of the photon and the creation of an electron-pair; this phenomenon is referred to as the Pair Production Effect.

A brief discussion of these four microscopic phenomena, and their macroscopic attenuating effect on a beam of photons, follows under the headings:

- A) Photoelectric Effect
- B) Compton Scattering
- C) Rayleigh Scattering
- D) Pair Production
- E) Attenuation

### A. Photoelectric Effect

At relatively low photon energies the most probable effect of an interaction is absorption of the incident photon by an electron of the traversed medium followed by ejection of that electron and emission of either characteristic X-rays or "Auger electrons" as explained below. This phenomenon, called the Photoelectric Effect, results in the complete disappearance of the incident photon<sup>(23)</sup>.

In order that total absorption may take place, and momentum be conserved, the interacting electron must be initially bound, in which case the residual atom recoils. The most tightly-bound electron, with respect to the incident photon energy, has the greatest probability of absorbing the photon. The interaction cross-section is a maximum when the photon energy  $E_\gamma$ , is just equal to the electron binding energy; it decreases gradually as  $E_\gamma$  increases, and decreases sharply as  $E_\gamma$  decreases. The most tightly-bound electron in an atom is in the K-shell; it accounts for in excess of 80% of the photoelectric absorptions, with the L-shell accounting for most of the remainder. The energy of the ejected electron, or photoelectron as it is usually called, is given by:

$$E_e = h\nu_o - E_{eb}, \text{ (MeV)} \quad (1)$$

where

$h\nu_o$  = incident photon energy (MeV).

$E_{eb}$  = electron binding energy (MeV).

The energy  $E_{eb}$  is carried away from the atom by radiation emitted as the inner shell vacancy is filled by an outer shell electron, such radiation is referred to as Characteristic X-rays. If the X-rays interact with an outer shell electron as they leave the atom, they will be absorbed and the absorbing electron emitted instead -- an Auger electron. The nuclear decay processes of internal conversion and electron capture may also

lead to the emission of characteristic X-rays; so also will the absorption of beta particles.

The photoelectric effect does not lend itself easily to explicit theoretical calculation. Determinations of its cross-sections are usually based on a combination of empirical treatments which vary according to the energy range under consideration. It is the practice of most researchers to make use of tabulations for  $\sigma_{PE}$ , the photoelectric cross-section<sup>(17-21)</sup>.

### B. Compton Scattering Effect

As the wavelength of gamma photons decrease and their photon energy increases, their behaviour tends towards that of a particle and their identity with a wave diminishes. The region of this transition corresponds to the Compton scattering "threshold." This threshold, not sharply-defined, is entered upon gradually as  $h\nu_0 \rightarrow m_0 c^2$ , ( $= 0.51 \text{ MeV}$ ), where  $m_0$  equals the rest mass of the electron. Viewed as solid bodies, the photon and the electron have comparable "masses." As the Compton effect becomes significant, the photoelectric effect significance diminishes<sup>(23)</sup>.

Compton scattering may be considered as an inelastic collision between an incident photon and a "free" electron of the medium; the collision is analogous to that of billiard ball mechanics. The electron may be thought of as free to recoil on the basis of  $h\nu_0 \gg E_{eb}$ , as a result of which the incident photon may transfer a portion of its momentum and energy. The consequence of the collision is a scattered photon of energy  $h\nu_1$ , travelling in a new direction and at an angle  $\theta$  with the original photon direction, and a recoiling electron of energy  $E_e$  making an angle  $\psi$  with the incident photon direction.  $\theta_{\text{max}} = 180^\circ$ ;  $\psi_{\text{max}} = 90^\circ$ .

The angular and energy relationships of these statements may be expressed as:

$$E_{\gamma_1} = \frac{E_{\gamma_0}}{1 + \frac{E_{\gamma_0}}{m_0 c^2} (1 - \cos \theta)}, \text{ MeV.} \quad (2)$$

$$E_e = E_{\gamma_0} - E_{\gamma_1} \quad (3)$$

$$E_{\gamma} = h\nu, \text{ MeV.} \quad (4)$$

$$\cot \psi = (1 + \alpha'_0) \tan \frac{\theta}{2} \quad (5)$$

where

$E_{\gamma_0}$  = incident photon energy, MeV.

$E_{\gamma_1}$  = scattered photon energy, MeV.

$\theta$  = angle between incident and scattered photon directions.

$\psi$  = angle between incident photon and recoil electron directions.

For convenience in the remainder of this section the following conventional short form is used:

$$\alpha'_0 = \frac{E_{\gamma_0}}{m_0 c^2}, \quad \alpha'_1 = \frac{E_{\gamma_1}}{m_0 c^2} \quad (6)$$

The differential "collision" cross-section for the scattering of photons into a given solid angle  $d\Omega$  at a particular angle  $\theta$  is given by the Klein-Nishina formula<sup>(23)</sup>, as

$$d\sigma = \frac{r_e^2}{2} d\Omega \left\{ \frac{(1 + \cos^2 \theta)}{[1 + \alpha'_0(1 - \cos \theta)]^2} \right\} \times \left\{ 1 + \frac{\alpha'^2_0 (1 - \cos \theta)^2}{(1 + \cos^2 \theta) [1 + \alpha'_0(1 - \cos \theta)]} \right\} \quad (7)$$

where

$$\begin{aligned} d\sigma &= \text{differential cross-section, cm}^2/\text{electron} \\ d\Omega &= 2\pi \sin \theta d\theta, \text{ the differential solid angle} \\ r_e &= \text{"classical electron radius, } \frac{e^2}{m_o c^2} \\ &= 2.818 \times 10^{-13} \text{ cm.} \end{aligned}$$

Equation (7) assumes the incident photons to be unpolarized. It indicates that for large  $\alpha'_0$ , scattering is predominantly in the forward cone. As  $\alpha'_0 \rightarrow 0$ , and  $\cos \theta \rightarrow 1$ , we see

$$d\sigma \rightarrow \frac{r_e^2}{2} (1 + \cos^2 \theta) d\Omega \quad (8)$$

From Equation (2) equation (7) may be rewritten in terms of energy

$$\frac{d\sigma}{d\alpha'_1} = \frac{\pi r_e^2}{\alpha'^2_0} \left\{ \frac{2}{\alpha'_0} - \frac{2}{\alpha'_1} + \frac{1}{\alpha'^2_0} + \frac{1}{\alpha'^2_1} - \frac{2}{\alpha'_0 \alpha'_1} + \frac{\alpha'_0}{\alpha'_1} + \frac{\alpha'_1}{\alpha'_0} \right\} \quad (9)$$

for

$$\alpha'_0 \geq \alpha'_1 \geq \frac{\alpha'_0}{(1 + 2\alpha'_0)}$$



The integration of Equation (9) over all scattered energies yields the total Compton scattering cross-section per electron,  $\sigma_{cs}$  , :

$$\sigma_{cs} = 2\pi r_e^2 \left\{ \frac{1 + \alpha'_o}{\alpha_o'^3} \left[ \frac{2\alpha_o'(1 + \alpha_o')}{1 + 2\alpha_o'} - \ln(1 + 2\alpha_o') \right] + \frac{\ln(1 + 2\alpha_o')}{2\alpha_o'} - \frac{1 + 3\alpha_o'}{(1 + 2\alpha_o')^2} \right\} \quad (10)$$

The total Compton scattering cross-section per atom is given by  $Z \cdot \sigma_{cs}$  , where Z is atomic number.

### C. Rayleigh Scattering Effect

In Compton scattering the atomic electrons are assumed to be unbound. This assumption is only valid at photon energies which are large with respect to the electron binding energy. A low energy photon may be elastically scattered by a tightly bound atomic electron, with the atom as a whole absorbing the recoil momentum. A bound electron has a "mass" which is equivalent to that of its atom. The energy transferred to the atom is small, and so the scattered photon proceeds with a relatively unaltered energy and only a slightly altered direction. This effect is known as the Rayleigh or small-angle scattering effect.

Since all the electrons in a given atom behave similarly, Rayleigh scattering is coherent. Because all the atoms of a given solid may be packed regularly, the effect may extend to the electrons of different atoms. When the scattering angle,  $\theta_R \approx 0$ , the scattering will be in phase, i.e. constructive interference. As  $\theta_R$  increases the tendency

The integration of Equation (9) over all scattered energies yields the total Compton scattering cross-section per electron,  $\sigma_{cs}$  , :

$$\sigma_{cs} = 2\pi r_e^2 \left\{ \frac{1 + \alpha'_o}{\alpha_o'^3} \left[ \frac{2\alpha'_o(1 + \alpha_o'')}{1 + 2\alpha'_o} - \ln(1 + 2\alpha'_o) \right] + \frac{\ln(1 + 2\alpha'_o)}{2\alpha'_o} - \frac{1 + 3\alpha'_o}{(1 + 2\alpha'_o)^2} \right\} \quad (10)$$

The total Compton scattering cross-section per atom is given by  $Z \cdot \sigma_{cs}$  , where Z is atomic number.

### C. Rayleigh Scattering Effect

In Compton scattering the atomic electrons are assumed to be unbound. This assumption is only valid at photon energies which are large with respect to the electron binding energy. A low energy photon may be elastically scattered by a tightly bound atomic electron, with the atom as a whole absorbing the recoil momentum. A bound electron has a "mass" which is equivalent to that of its atom. The energy transferred to the atom is small, and so the scattered photon proceeds with a relatively unaltered energy and only a slightly altered direction. This effect is known as the Rayleigh or small-angle scattering effect.

Since all the electrons in a given atom behave similarly, Rayleigh scattering is coherent. Because all the atoms of a given solid may be packed regularly, the effect may extend to the electrons of different atoms. When the scattering angle,  $\theta_R \approx 0$ , the scattering will be in phase, i.e. constructive interference. As  $\theta_R$  increases the tendency

is towards destructive interference and so the scattered photons will be found concentrated mainly in a narrow forward cone, and to a lesser extent in other discrete directions. This may be realized from consideration of the photon wavelength, and the atomic radius, analogous to Bragg reflection<sup>(24)</sup>. This behaviour differs from Compton scattering, where the independence of the electrons precludes the likelihood of interference.

The transition from Rayleigh scattering to Compton scattering is smooth with increasing energy,  $E_{\gamma_0}$ . The Rayleigh scattered photon does not have a unique energy as a function of scattering angle, having instead an energy distribution peaked at a value close to that given by Equation (2).

#### D. Pair Production Effect

At photon energies of approximately 1.0 MeV the predominant interaction phenomenon is Compton scattering. As  $E_{\gamma_0}$  is increased considerably above this energy the photon may interact with the electric field surrounding either a nucleus or an electron. The photon will be absorbed and replaced by a pair of electrons, a positron and a negative electron. This effect is called Pair Production.

The cross-section for pair production in the field of an orbital electron is negligible until  $E_{\gamma_0} \geq 4 m_0 c^2$ , (= 2.04 MeV). Nuclear pair production, however, has a cross-section which begins at the photon threshold energy  $2 m_0 c^2$ , (= 1.02 MeV), and increases rapidly thereafter.

The electron pair share and carry away the energy in excess of that required for their creation, as kinetic energy; this may be expressed as

$$(E_{e-} + E_{e+}) = E_{\gamma_0} - 2m_0c^2 \quad (11)$$

The free positron is quickly annihilated by a negative electron after its kinetic energy has been dissipated. The annihilation yields a randomly oriented pair of back-to-back photons, each with an energy of  $m_0c^2$ .

The electron pair are distributed mainly in the forward direction with the average angle of "deflection" being expressed by  $m_0c^2/E_e$ .

For  $2m_0c^2 < E_{\gamma_0} < 4m_0c^2$ ,  $\sigma_{pp} \propto Z^2$ .

#### E. Attenuation

The passage of a beam of photons through a medium is characterized by their interactions with the atoms of that medium. This leads to a reduction in the number of uncollided primary photons at a depth. The reduction is referred to as the attenuation of the incident photon number<sup>(2,23,24)</sup>.

The discussion on interactions has shown that the total microscopic energy dependent cross-section for a particular interaction process occurring, is given by either  $\sigma_{PE}$ ,  $Z\sigma_{CS}$ ,  $\sigma_{RS}$  or  $\sigma_{PP}$ . The total cross-section  $\sigma_{TOT}(E_{\gamma_0})$ , for "some" process occurring, is then given by the sum of the partial cross-sections as

$$\sigma_{TOT}(E_{\gamma_0}) = \sigma_{TOT} = \sigma_{PE} + Z\sigma_{CS} + \sigma_{RS} + \sigma_{PP}, \text{ (cm}^2\text{/atom)} \quad (12)$$

from which a total macroscopic cross-section per cm of path may be defined as

$$\mu_{TOT}(E_{\gamma_0}) = \mu_{TOT} = N\sigma_{TOT}, \text{ (cm}^{-1}\text{)} \quad (13)$$

$$(E_{e^-} + E_{e^+}) = E_{\gamma_0} - 2m_0c^2 \quad (11)$$

The free positron is quickly annihilated by a negative electron after its kinetic energy has been dissipated. The annihilation yields a randomly oriented pair of back-to-back photons, each with an energy of  $m_0c^2$ .

The electron pair are distributed mainly in the forward direction with the average angle of "deflection" being expressed by  $m_0c^2/E_e$ .

For  $2m_0c^2 < E_{\gamma_0} < 4m_0c^2$ ,  $\sigma_{pp} \propto Z^2$ .

#### E. Attenuation

The passage of a beam of photons through a medium is characterized by their interactions with the atoms of that medium. This leads to a reduction in the number of uncollided primary photons at a depth. The reduction is referred to as the attenuation of the incident photon number<sup>(2,23,24)</sup>.

The discussion on interactions has shown that the total microscopic energy dependent cross-section for a particular interaction process occurring, is given by either  $\sigma_{PE}$ ,  $Z\sigma_{CS}$ ,  $\sigma_{RS}$  or  $\sigma_{PP}$ . The total cross-section  $\sigma_{TOT}(E_{\gamma_0})$ , for "some" process occurring, is then given by the sum of the partial cross-sections as

$$\sigma_{TOT}(E_{\gamma_0}) = \sigma_{TOT} = \sigma_{PE} + Z\sigma_{CS} + \sigma_{RS} + \sigma_{PP}, \text{ (cm}^2\text{/atom)} \quad (12)$$

from which a total macroscopic cross-section per cm of path may be defined as

$$\mu_{TOT}(E_{\gamma_0}) = \mu_{TOT} = N\sigma_{TOT}, \text{ (cm}^{-1}\text{)} \quad (13)$$

and similarly

$$\mu_{PE} = N\sigma_{PE} ; \mu_{CS} = NZ\sigma_{CS} ; \mu_{RS} = N\sigma_{RS} ; \mu_{PP} = N\sigma_{PP} \quad (14)$$

where

$$N = \frac{\rho \times A_V}{M} ; \text{ (atoms present/cc) } \quad (15)$$

assuming one type of atom only.

$\rho$  = density of medium, (gm/cc).

$A_V$  = Avogadro number, (atoms/mole);  $6.023 \times 10^{-23}$

$M$  = atomic or molecular weight.

The inverse of Equation is defined as the mean free path,  $\ell_{TOT}$ , for a photon prior to interaction, i.e.

$$\ell_{TOT} = \frac{1}{\mu_{TOT}} , \text{ (cm) } \quad (16)$$

Similarly  $\ell_{RE}$ ,  $\ell_{CS}$ ,  $\ell_{RS}$ , and  $\ell_{PP}$  may be defined from Equation (14).

The total macroscopic cross-section is generally referred to as the total linear attenuation coefficient.

The number of normally incident photons per  $\text{cm}^2$ -sec in a parallel beam which penetrate a thickness  $x$  of a homogeneous medium without interaction, is given by the exponential law as

$$\phi(x) = \phi(0)e^{-\mu x} \text{ (}\gamma/\text{cm}^2\text{-sec)} \quad (17)$$

where

$\phi(0)$  = number of photons/ $\text{cm}^2$ -sec incident at  $x=0$ .

$\phi(x)$  = number of photons/ $\text{cm}^2$ -sec emerging at  $x$ .

$\mu$  = cross-section appropriate to the interaction effect under consideration; energy dependent.

Thus, it follows that the probability of uncollided photon transmission through a thickness  $x$  is given by  $p$ , where

$$p = \frac{\phi(x)}{\phi(0)} = e^{-\mu_{TOT}x} \quad (18)$$

Equation (18) is in agreement with Equation (4) of Report-Section (2.2).

Similarly the probability of some kind of interaction occurring in path length  $x$  is given by

$$\epsilon_{TOT}(x) = (1 - p) = (1 - e^{-\mu_{TOT}x}) \quad (19)$$

Equations , and assume a normally incident parallel or collimated, photon beam. In practice this can only be nearly achieved by narrow-geometry restrictions. For the case of a poorly collimated or uncollimated photon beam it is necessary to introduce a factor to express the increase of the photon number flux at  $x$  over the value predicted by Equation (3.4.17). This factor, known as a number Build-Up Factor,  $B(x)$ , may be defined as <sup>(2,3,24)</sup>

$$B(x) = \frac{\text{Total Number Flux at } x}{\text{Uncollided Flux at } x} \geq 1.0 \quad (20)$$

which is in agreement with Equation (5) of Report-Section (2.2)

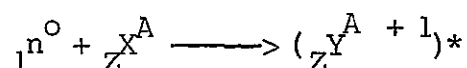
Energy and dose build-up factors may be similarly defined.

That  $\mu$  is a function of both incident photon energy,  $E_{\gamma_0}$ , and the properties of the traversed medium is apparent from the discussions of sub sections (A-D) and equations (12) to (15). It follows then, that any property, including  $B(x)$  which is dependent on  $\mu$ , is similarly dependent on  $E_{\gamma_0}$ .

## II FAST NEUTRON INTERACTION PHENOMENA

Neutrons interact with the nuclei of traversed matter through the mechanism of nuclear force. An interaction is generally referred to as either having scattered or absorbed the incident neutron. The probability of either scattering or absorption varies as a function of the incident photon energy and the atomic number of the target nuclide, the dependence on atomic number being general and such that for each isotope there is a unique probability, or cross-section<sup>(2,28,29)</sup>.

Perhaps the most convenient and systematic manner of describing neutron interactions consists of invoking the "compound nucleus" concept. According to this concept all interaction modes result in the formation of an intermediate reaction product - a compound nucleus - formed by an absorption of the incident neutron. Symbolically this may be represented as



where,  ${}_1^0\text{n}$  is the incident neutron,  ${}_Z^A\text{X}$  the target nucleus before interaction and  ${}_Z^{A+1}\text{Y}$  the compound nucleus formed by the interaction. The asterisk denotes that the compound nucleus will, in general, be left in an excited state for a finite period of time. The energy of the compound nucleus includes both the binding energy and/or part of the kinetic energy of the incident neutron. This energy excess over that of  ${}_Z^A\text{X}$ , distributed in a complex fashion among the nucleons, will cause the compound nucleus system to seek its state of lowest permissible energy in a characteristic "relaxation time", typically about  $10^{-20}$  to  $10^{-12}$  seconds.

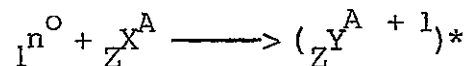
The laws of quantum mechanics allow only those reactions to take place which obey certain rigid energy and momentum relationships. This obedience is observed with respect to the available excitation energy of the incident neutron and the distribution of energy levels in the target nucleus, as well as with respect to the symmetry requirements of the interaction,



## II FAST NEUTRON INTERACTION PHENOMENA

Neutrons interact with the nuclei of traversed matter through the mechanism of nuclear force. An interaction is generally referred to as either having scattered or absorbed the incident neutron. The probability of either scattering or absorption varies as a function of the incident photon energy and the atomic number of the target nuclide, the dependence on atomic number being general and such that for each isotope there is a unique probability, or cross-section (2,28,29).

Perhaps the most convenient and systematic manner of describing neutron interactions consists of invoking the "compound nucleus" concept. According to this concept all interaction modes result in the formation of an intermediate reaction product - a compound nucleus - formed by an absorption of the incident neutron. Symbolically this may be represented as



where,  ${}_1^0\text{n}$  is the incident neutron,  ${}_Z^A\text{X}$  the target nucleus before interaction and  ${}_Z^{A+1}\text{Y}$  the compound nucleus formed by the interaction. The asterisk denotes that the compound nucleus will, in general, be left in an excited state for a finite period of time. The energy of the compound nucleus includes both the binding energy and/or part of the kinetic energy of the incident neutron. This energy excess over that of  ${}_Z^A\text{X}$ , distributed in a complex fashion among the nucleons, will cause the compound nucleus system to seek its state of lowest permissible energy in a characteristic "relaxation time", typically about  $10^{-20}$  to  $10^{-12}$  seconds.

The laws of quantum mechanics allow only those reactions to take place which obey certain rigid energy and momentum relationships. This obedience is observed with respect to the available excitation energy of the incident neutron and the distribution of energy levels in the target nucleus, as well as with respect to the symmetry requirements of the interaction,

e. g. parity, baryon number, charge conservation, statistics.

In accord with the compound nucleus concept, scattering and absorption of an incident neutron may be defined in terms of whether or not the compound nucleus emits a neutron during de-excitation. Further and more important, scattering may be separated into two kinds - elastic and inelastic. In elastic scattering the compound nucleus emits a kinetic energy degraded neutron in a very short relaxation time  $< 10^{-20}$  seconds, and is itself left in exactly the same internal energy state as before the interaction. In inelastic scattering the compound nucleus emits a neutron of partially or totally degraded kinetic energy and is itself left in an internal energy state above that of  ${}^A_ZX$ ; the excess energy is evolved by emission of one or more gamma photons. The degradation of the neutron kinetic energy by scattering is referred to as thermalization. The compound nucleus may be de-excited by emission of particles other than neutrons, such as alphas and betas accompanied by gamma photons in which case neutron absorption is said to have resulted.

The interaction processes reviewed above are summarized:

(i) Elastic Scattering, (n,n)——A neutron of reduced kinetic energy is emitted by the short-lived compound nucleus which is left in an unexcited state. Kinetic energy is transferred to recoil the target nucleus. In the case of hydrogen target nuclei, for which energy transfer is a maximum, recoil protons result.

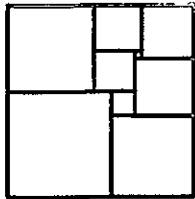
(ii) Inelastic Scattering, (n,n')——A neutron of reduced kinetic energy is emitted by the compound nucleus. The compound nucleus is de-excited by gamma photon emission.

(iii) Radiative Capture, (n, $\gamma$ )——The compound nucleus formed by absorption of an incident neutron is de-excited by relatively high energy gamma photon emission.

(iv) Charged Particle Emission, (n,p), (n,d), (n, $\alpha$ )——The compound nucleus formed by absorption of an incident neutron is de-excited by emission of a charged particle such as a proton, deuteron or alpha, accompanied by gamma photons.

(v) Fission, (n,f)——The compound nucleus formed by absorption of an incident neutron breaks into two ionizing fission fragments, and one or more energetic neutrons, accompanied by gamma photon emission. Fission is most probable in heavy nuclei of odd mass number and less so in heavy nuclei of even mass number. It can occur either as the result of an externally incident neutron or as a consequence of quantum mechanical leakage through the Coulomb barrier, ie., spontaneous fission.

(vi) Other Reactions, ( $\alpha$ ,n), ( $\gamma$ ,n)——Two interaction processes which give rise to neutron emission and thus which must be identified are ( $\alpha$ ,n) and ( $\gamma$ ,n) phenomena in the plutonium-oxide source and its immediate environment. The first reaction proceeds when the energy of an alpha particle exceeds the energetic threshold and Coulomb repulsion barrier for the reaction, and is thus significant only for plutonium alphas ( $\sim 5.5$  MeV) incident on light-target nuclei such as beryllium. The second reaction, photo-neutron formation, results from the interaction of high energy gamma photons with light nuclei such as are present in plutonium-oxide as impurities. High energy photons are present in the PuO<sub>2</sub> source through (n,f) reactions and the decay of the Tl<sup>208</sup> daughter of the Pu<sup>236</sup> isotope present in plutonium oxide.



**NUS CORPORATION**